

# Harvest-and-Opportunistic-Relay: Analyses on Transmission Outage and Covertness

Yuanjian Li, Rui Zhao, *Member, IEEE*, Zhiqiao Nie and A.

Hamid Aghvami, *Fellow, IEEE*

## Abstract

For enhancing transmission performance, privacy level and energy manipulating efficiency of wireless networks, this paper initiates a novel simultaneous wireless information and power transfer (SWIPT) full-duplex (FD) relaying protocol, termed harvest-and-opportunistic-relay (HOR). In the proposed HOR protocol, the relay can work opportunistically in either pure energy harvesting (PEH) or the FD SWIPT mode. Due to the FD characteristics, the dynamic fluctuation of R's residual energy is difficult to quantify and track. To solve this problem, we apply a novel discrete-state Markov Chain (MC) method in which the practical finite-capacity energy storage is considered. Furthermore, to improve the privacy level of the proposed HOR relaying system, covert transmission performance analysis is developed and investigated, where closed-form expressions of optimal detection threshold and minimum detection error probability are derived. Last but not least, with the aid of stationary distribution of the MC, closed-form expression of transmission outage probability is calculated, based on which transmission outage performance is analyzed. Numerical results have validated the correctness of analyses on transmission outage and covert communication. The impacts of key system parameters on the performance of transmission outage and covert communication are given and discussed. Based on mathematical analysis and numerical results, it is fair to say that the proposed HOR model is able to not only reliably enhance the transmission performance via smartly managing residual energy but also efficiently improve the privacy level of the legitimate transmission party via dynamically adjust the optimal detection threshold.

Yuanjian Li and A. Hamid Aghvami are with Centre for Telecommunications Research (CTR), King's College London, London WC2R 2LS, U.K. (e-mail: yuanjian.li@kcl.ac.uk; hamid.aghvami@kcl.ac.uk).

Rui Zhao and Zhiqiao Nie are with Xiamen Key Laboratory of Mobile Multimedia Communications, Huaqiao University, Xiamen 361021, China. (e-mail: rzhao@hqu.edu.cn; zqnie@hqu.edu.cn).

This work has been submitted to the IEEE for possible publication. Copyright may be transferred without notice, after which this version may no longer be accessible.

## I. INTRODUCTION

### A. Background

Conventionally, wireless communication systems are basically powered by rechargeable battery or electrical grid, such as cellular, Bluetooth, Wi-Fi and sensor networks. There are several distinguish physical or/and economic disadvantages rooted in these traditional wireless communication power supply methods, which has been the bottleneck restricting the ubiquitous applications of wireless communication [1]. More precisely stated, grid-powered wireless communication systems, e.g., cellular networks, require solid support of electrical grid infrastructure, which may not only need much more construction resources but also lead to enormous energy consumption; The operational lifetime of battery-powered wireless networks is usually limited, for finite battery capacity in practical applications, leading to periodic battery replacement or recharging. To prolong the wireless networks lifetime and improve the energy efficiency, the research of energy-aware architectures and transmission strategies has been a hotspot in recent years.

Energy harvesting (EH) technique is able to scavenge energy from natural resources (e.g., solar power, piezoelectric energy, wind and mechanical vibrations), which is known as a promising candidate to overcome the aforementioned disadvantages of the traditional power supply strategies. Unfortunately, the amount of energy harvested from natural resources highly depends on several uncontrollable factors, such as the weather condition, resulting in EH unreliability. To aid this, a promising method scavenging energy from man-made radio frequency (RF) radiation has gained lots of research concentrations [2]. Inspired by the fact that the RF signals can carry the intended information and energy at the same time, the concept of simultaneous wireless information and power transfer (SWIPT) was coined in [3]. Thereafter, two practical SWIPT strategies were introduced in [4], i.e., time-switching (TS) and power-splitting (PS) based SWIPT, in which the missions of information decoding (ID) and EH are conducted respectively in time or power domain. Specifically, the TS-based method allocates part of the time slot to decode information and the remaining to harvest energy, whereas one portion of the received signal power is utilized for ID and the other portion is used for EH in the PS-based strategy [5]. Based on these practical SWIPT strategies, various essential issues about SWIPT were studied in different wireless transmission systems, e.g., maximizing the ergodic rate for a dynamic SWIPT approach in the cooperative cognitive radio network (CCRN) [6], a non-cooperative game theoretic approach for the resource optimization in SWIPT enabled heterogeneous small

cell network (HetSNet) [7], optimizing the energy efficiency (EE) by delicately designing the precoders at the transceivers in the multiple-input multiple-output (MIMO) two-way wireless networks [8].

Full-duplex (FD) technology which allows transceivers emit and receive information simultaneously, can potentially achieve efficient utilization of wireless resources (say, time and frequency), and thus it is expected to overcome the shortcomings of half-duplex (HD) counterpart on spectral efficiency (SE) [9]. However, the theoretical performance of FD nodes is significantly limited by the harmful self-interference (SI) which represents that the emitted signals may be directly/indirectly received by their own receivers at the FD nodes [10]. Fortunately, thanks to recent advances in SI cancellation (SIC) techniques (e.g., passive and active SIC approaches), it is possible to suppress the SI to noise level, which makes the FD technology more practical and feasible in practice [11], [12]. Nevertheless, due to the RF impairments, SI cannot be restrained perfectly so that the FD networks are still impacted by the so-called residual SI (RSI) [13].

Thereafter, FD technique has drawn attention from both academic and industrial communities. Among various wireless FD transmission applications, one popular candidate is the FD relaying (FDR) technique, which can not only extend the transmission coverage and combat the severe fading in wireless communications but also enhance the utilization efficiency of wireless resources [14]. Some of the corresponding works have coped with the performance of various FDR network backgrounds, in the presence of RSI. For example, two buffer-aided relaying approaches with adaptive transmission-reception at the FD relay in the absence of direct link between the source and the destination were proposed and studied in [15]; whereas the outage probability of an amplify-and-forward (AF) FDR network with direct source-destination link was investigated in [16]. Moreover, in the case of decode-and-forward (DF) relaying protocol, [17] researched the ergodic achievable secrecy rate issue in the FDR wiretap channels.

With rapid development of the fifth-generation (5G) wireless networks and Internet of Things (IoT), rocketing sorts and amounts of private information (e.g., location data, control orders, social identity information, e-health indexes) are needed to be shared wirelessly among transceivers. Consequently, growing concerns have been posing on security and privacy (low detection probability by the third party) of wireless transmissions. In the existing literature, security issues of wireless communications are much more concerned and investigated than its privacy counterpart. To enhance wireless information security, lots of works have been developed, like, cryptography and information-theoretic physical layer security techniques. However, the

inherently public and visible nature of wireless medium (electromagnetic wave) not only leads to the security vulnerability but also privacy weakness. Recently, increasing research efforts have been pouring into the field of low probability of detection on the existence of wireless transmissions, namely, covert communications. For example, communicating covert messages under the detection of legitimate party who does not desire the leakage of sensitive information which is supposed to be kept confidential within authorized transceivers, belongs to covert communication research regime. The famous Square Root Law which indicates the fact that  $\mathcal{O}(\sqrt{n})$  bits of information can be transmitted reliably and covertly in  $n$  channel uses over additive white Gaussian noise (AWGN) channels as  $n \rightarrow +\infty$ , was coined in [18]. Afterwards, covert transmissions have been researched and investigated in various wireless communication scenarios [19]–[21]. In [19], the authors studied covert wireless communications in the presence of a FD receiver which can generate artificial noise to cause uncertainty at the adversary so that low probability of detection can be achievable. Considering both centralized and distributed antenna systems (CAS/DAS), multi-antenna-aided covert communications coexisting with randomly located wardens and interferers was studied in [20]. Authors of [21] jointly optimized trajectory and transmit power for covert transmission in unmanned aerial vehicle (UAV) networks, aiming to hide a UAV for communicating critical informations.

### *B. Related Works and Motivation*

Hereby, we review the related works, point out the differences and claim our motivation.

It has been a promising solution to meet the green communication and the reliable transmission demand in the upcoming 5G and IoT era by introducing SWIPT into FDR wireless communications. Particularly, in the scenario which contains power-constrained relay node, the SWIPT FDR has the potential to not only solve power supply problem but also enhance significantly key wireless transmission performances, like, reliability, SE, valid coverage, quality of service (QoS), etc. Besides, by delicately designing the covert communication detection strategy, it is promising to improve privacy level of the SWIPT FDR system.

To the best of the authors' knowledge, there already exist inspiring related literature which investigated and studied SWIPT FDR in the context of different wireless network setups. In [22], the characteristics and performance of PS-based two-way SWIPT FDR networks as well as the relay selection issue were researched. In [23], a joint optimization method finding the source as well as the relay beamformers was proposed and the numerical results for the mean squared

error (MSE) and bit error rate (BER) showed that the proposed method performed well in the MIMO SWIPT FDR systems. In [24], the throughput maximization problem for a FDR wireless communication network with simultaneous down-link energy transfer and up-link information transmission was investigated. In [25], outage probability and average throughput performances were investigated in a SWIPT FDR wireless network. Unfortunately, the aforementioned works and the majority of existing literature on SWIPT FDR did not include the consideration on covert communications. To bridge this research gap, we investigate covert communication problems of SWIPT FDR systems in this paper.

Regarding the related works of covert communications in the field of wireless relaying networks, it is still in its infancy stage. In [26], Hu *et al.* examined the possibility, performance limits, and associated costs for a power-constrained HD relay transmitting covert information on top of forwarding the source's information. Wang *et al.* [27] investigated how channel uncertainty can influence covert communication performance in wireless relaying networks. A covert communication scheme under fading channels was proposed and studied in [28] where the relay not only forwards source's information but also plays the role as a cooperative jammer. However, so far, discrete EH technique has not been considered in the existing literature regarding covert communications, which is a main concern of this paper.

Motivated by the aforementioned contents, we propose a novel wireless relaying protocol in which discrete-energy-state SWIPT FDR and covert communications are combined and considered, aiming to enhance wireless transmission performance while improving its privacy level.

### C. Our Contributions

In this paper, a new transmission protocol termed harvest-and-opportunistic-relay (HOR) is designed and analyzed. Specifically, the FD relay which contains no sustainable power supply but wireless EH system and rechargeable energy storage is deployed to opportunistically help the source and the destination complete their wireless communication. In the proposed HOR protocol, according to the relay's energy status and channel condition between the source and the destination, the relay works dynamically in either pure energy harvesting (PEH) or the FD SWIPT mode. Furthermore, to evaluate the detection performance on potential covert communication, i.e., improving the privacy level of the proposed HOR protocol, performance analysis on covert transmission is developed and investigated. As far as the authors know, we are the first to

introduce both discrete EH and covert communications into SWIPT FDR systems. The main contributions of the paper are concluded in details as follows.

- *Protocol Design*: We systematically establish a novel HOR protocol from listing necessary hardware facilities to designing feasible transmission strategy. The proposed HOR scheme can efficiently enhance wireless transmission performance between the source and the destination, via flexibly managing the relay's precious stored energy. Besides, through covert communication analysis, privacy level of the proposed HOR system can be improved. It is fair to claim that the proposed HOR scheme is able to not only enhance wireless transmission performance but also improve the system's privacy level.
- *Hybrid Energy Storage and Markov Chain*: We consider the practical energy storage model under the limitation of finite capacity at the relay. To enable the relay's FD functionality, a hybrid energy storage scheme is adopted, which consists of both primary and secondary energy storages. To track dynamic fluctuation of residual energy, energy discretization and discrete-state MC method is applied to model the complicated energy state transitions. It is worth noting that all the transition probabilities are calculated in closed-form. Then, the stationary distribution of the MC is given.
- *Covert Communication Analysis*: Under the cover of forwarded source messages, there exists potential threat of critical information leakage. To improve the HOR protocol's privacy level, we provide covert communication analysis given channel uncertainty in this paper. The optimality of radiometer for covert message detection is proved. Closed-form expressions of false alarm and missed detection probabilities are derived, based on which we calculate closed-form expressions of the optimal detection threshold and the corresponding minimum detection error probability. Furthermore, the impacts of imperfect channel estimation on the minimum detection error probability is also discussed.
- *Transmission Performance Analysis*: Invoking the MC's stationary distribution, closed-form expression of transmission outage probability is derived, then we provide transmission outage analysis of the proposed HOR scheme. Furthermore, the impacts of key system parameters on transmission outage performance are investigated via numerical results.

#### D. Outline and Notation

*Organization*: The paper is organized as follows. Section II presents the HOR model and its transmission strategy. Section III describes the energy discretization, detailed derivation on the

MC and the stationary distribution. Section IV shows covert communication analysis. Section V gives transmission outage performance analysis. Simulation results are presented in Section VI and conclusions are drawn in Section VII.

*Notation:* Bold lower case letters denote vectors, e.g.,  $\mathbf{v}$ . Bold upper case letters denote matrices, e.g.,  $\mathbf{M}$ .  $(\cdot)^T$ ,  $(\cdot)^{-1}$ ,  $\mathbf{I}$  indicate transpose of matrix, inverse of matrix, unit matrix, while  $\mathbb{E}\{\cdot\}$  and  $|\cdot|$  mean statistical expectation and modulo operators of a complex number, respectively.  $\mathcal{CN}(\mu, \sigma^2)$  stands for the complex Gaussian distribution with mean  $\mu$  and variance  $\sigma^2$ . The intersection of two sets  $A$  and  $B$  is denoted by  $A \cap B$ .  $\Pr(\cdot)$  is the operator calculating probability of a specific objective. Symbols  $\sum$  and  $\prod$  represent the summation and product operations of a sequence of terms, respectively.

## II. SYSTEM MODEL AND TRANSMISSION STRATEGY

A classical three-node wireless relaying network, which comprises one source (S), one destination (D) and one relay (R), is considered in this paper. Energy-constrained R is equipped with dual antenna so that it can adopt the FD technique, whereas S and D are both single-antenna node. The novel HOR protocol is coined originally to assist wireless communication from S to D, with the ability of managing RF energy smartly, while improving the overall privacy level.

### A. Assumptions Regarding Wireless Channels

In this paper, we assume that all wireless channels are modeled as quasi-static Rayleigh fading channels, which means that these fading channels remain static within each transmission slot, and vary independently over different transmission slots. The Rayleigh fading distribution that the self-interference (SI) channel at R follows is considered because the line-of-sight (LoS) component can be largely eliminated via antenna isolation and the scattering plays the principal role herein. Note that the aforementioned slot is equivalent to a block of time over which the intended messages are transmitted. Besides, this paper considers the widely used infinite block-length model which means that each transmission slot is composed of  $n$  symbols and  $n \rightarrow \infty$  is assumed. Moreover, the block boundaries in wireless links are predefined to be synchronized perfectly throughout the whole system. Without loss of generality, the block duration in the considered model is normalized to one time unit so that the measures of power and energy are identical and can be used interchangeably in this paper. Wireless channels  $S \rightarrow D$ ,  $S \rightarrow R$ , and  $R \rightarrow D$  are denoted as  $h_{SD}$ ,  $h_{SR}$ , and  $h_{RD}$ , respectively. Moreover,  $h_{RR}$  indicates the SI link caused by the

FD characteristic at R. It is worth noting that the channel coefficients  $h_{SD}$ ,  $h_{SR}$ ,  $h_{RD}$  and  $h_{RR}$  are manipulated to encompass the gains of transmit and receive antennas as well as the path losses caused by propagation distances among the nodes in this paper. The aforementioned wireless channel coefficients follow independently and identically distributed (i.i.d.) complex Gaussian distribution with zero means and variance  $\mathbb{E}\{|h_{SD}|^2\} = \Omega_{SD}$ ,  $\mathbb{E}\{|h_{SR}|^2\} = \Omega_{SR}$ ,  $\mathbb{E}\{|h_{RD}|^2\} = \Omega_{RD}$  and  $\mathbb{E}\{|h_{RR}|^2\} = \Omega_{RR}$ .

Regarding the availability of global CSIs, the instantaneous CSI of channel between S and D are assumed to be available at S via channel estimation, but D can only gain the imperfect instantaneous CSI estimation of wireless channel between R and D. We note hereby that the availability of instantaneous S→R and R→R CSIs poses no influence on the considered performance analyses so that we do not rise any assumption on their availabilities.

### B. Relay Model

In the considered system model, R is known publicly to be energy-limited, leading to rigorous power supply problem which is expected to be solved by the promising SWIPT technique. Different from the traditional relay strategy, in this paper, a novel relay protocol named HOR is proposed, which allows R to work in either the PEH mode or the FD SWIPT mode opportunistically. In specific, when performing the FD SWIPT, R receives and forwards information simultaneously to assist the wireless transmission between S and D, while the PS-based EH solution is applied to harvest the RF energy. In the case of adopting the PEH mode, R concentrates on capturing wireless energy from the RF signals without any information processing. Apart from assisting wireless transmission, R is considered as potential leaker who intends to leak vital information regarding the source signals to the third party, which should keep covert from the legitimate party, i.e., S and D. The malicious intention of R keeps secrecy and the legitimate party cannot make sure whether R is innocent or not, the legitimate party treats R as an innocent and friendly node initially but keeps an eye on R detecting the potential covert communication generated by R.

For achieving the proposed HOR functionality, R should equip the following hardwares:

- 1) Three RF chains, enabling the EH, information forwarding and covert message emitting.
- 2) One rectifier utilized to transform the RF signals into direct currents (DC).
- 3) A battery serving as the principal energy carrier (PEC) with high energy capacity.
- 4) One minor battery (MB) for storing harvested energy temporarily, e.g., a capacitor.



5) A constant energy supply for sending covert message, whose existence is unaware publicly.

In details, the receive antenna at R is permanently bounded with the rectifier via one RF chain. One single battery cannot be charged and discharged simultaneously so that the FD SWIPT mode may not be realized, we herein apply both the PEC and the MB at R to crack this dilemma. Note that the PEC is directly connected to the rectifier and the transmitting RF chain for absorbing and releasing energy, respectively. In the PEH mode, the harvested energy are absorbed by the PEC directly. In the FD SWIPT mode, the PEC releases its residual energy to support the transmitting RF chain. Meanwhile, the MB stores the harvested energy temporarily and delivers all the stored energy into the PEC when the FD SWIPT mode terminates. The hidden constant energy supply which is connected to the other RF chain will release its power only when the relay decides to leak the system's informations.

Alongside assisting signal transmission between S and D, R is a rapacious node which intends to leak essential information (defined as the covert message herein) regarding the source signals, when the right opportunity occurs. The legal destination D also plays the role as a *warden* detecting the potential information leakage. Reducing the probability of being detected by the legitimate party, R would like to emit the covert message under some solid covers. In this proposed system, the forwarded version of the source signals is the only existing shield. Reasonably, R would consider the worst case (D can gain perfect channel estimation and know its own noise power) and intends to broadcast the covert message merely when itself works in the FD SWIPT mode. Otherwise, the covert communication initiated by R will be detected by D without any hesitation (i.e., probability one), which is definitely an undesired circumstance R ever expects. This is because, in the case of PEH, R is supposed to focus on EH without forwarding, any additional transmit power initiated at R will be detected easily by D.

### C. Transmission Protocol

In our proposed HOR protocol, before each transmission block is sent out, S broadcasts pilot signal to estimate  $h_{SD}$  which will be utilized to calculate the received instantaneous signal-to-noise-ratio (SNR) at D, denoted as  $\gamma_{SD} = P_S |h_{SD}|^2 / \sigma_D^2$  where  $P_S$  represents average transmit power at S,  $\sigma_D^2$  is the power of additive white Gaussian noise (AWGN) at D. In the case of  $\gamma_{SD} \geq \gamma_{th}$ , D feeds back two bits "11" to S through a feedback link, where  $\gamma_{th}$  is a predefined instantaneous SNR threshold. Otherwise, D feeds back two bits "00" instead. When S receives the feedback bits "11", S broadcasts two bits "01" to R. Otherwise (i.e., S receives "00"), S sends

out bits “10” alternatively. If R receives "01", it means the direct link between S and D is good enough so that R is not necessarily needed to assist the transmission between S and D, R keeps working in the PEH mode without forwarding any information (of course, including the possible covert message). If R receives bits “10”, which means the quality of received information at D is poor, R is expected to help the transmission from S to D. Before participating in transmission, R has to estimate its residual energy, checking whether the available energy is sufficient to support the transmission. If the energy state of R is greater than a given residual energy threshold  $E_{th}$ , i.e.,  $E_i \geq E_{th}$ , R feeds back bit “1” to S, otherwise, feeds back bit “0” instead. Once S receives the feedback bit “1” from R, S starts to broadcast the intended information signal, and R turns into the FD SWIPT mode, i.e., R helps S forward the information signal and harvests energy simultaneously. If S receives the feedback bit “0” from R, S broadcasts energy signal to charge the battery at R. At this very time, D ceases signal processing, because the energy signal is randomly generated by S and conveys no useful information.

The condition  $\gamma_{SD} \geq \gamma_{th}$  is referred as the “SNR requirement” which is applied to guarantee the reliability of communication from S to D. On the other hand, the condition  $E_i \geq E_{th}$  is regarded as the “energy requirement”, ensuring that the residual energy at R is sufficient to support the relying work.

We would like to explain the PEH and the FD SWIPT modes thoroughly in the following:

1) *The PEH Mode*: When R works in the PEH mode, R employs the reception antenna for receiving RF signals. Note that the PEH mode will be enabled in the case of either  $\gamma_{SD} \geq \gamma_{th}$  or  $\{\gamma_{SD} < \gamma_{th}\} \cap \{E_i < E_{th}\}$ . By ignoring the negligible energy harvested from the noise at the receiver, the total amount of energy harvested at R in a transmission slot can be given by

$$E_{PEH} = \eta P_S |h_{SR}|^2, \quad (1)$$

where  $\eta$  ( $0 < \eta < 1$ ) means the efficiency of energy conversion, and the harvested energy in this stage will be straight transferred into the PEC.

2) *The FD SWIPT Mode*: It is worth noting that the FD SWIPT mode will be invoked when the case  $\{\gamma_{SD} < \gamma_{th}\} \cap \{E_i \geq E_{th}\}$  holds. Only in this circumstance, R gets chance to broadcast covert message under the cover of the forwarded version of legitimate signals.

When R does not emit covert messages, the received signals at R and D can be expressed respectively as

$$\mathbf{y}_R[\omega] = \sqrt{P_S} h_{SR} \mathbf{x}_S[\omega] + \sqrt{k P_R} h_{RR} \mathbf{x}_R[\omega] + \mathbf{n}_R[\omega], \quad (2)$$

$$\mathbf{y}_D[\omega] = \sqrt{P_S}h_{SD}\mathbf{x}_S[\omega] + \sqrt{P_R}h_{RD}\mathbf{x}_R[\omega] + \mathbf{n}_D[\omega], \quad (3)$$

where  $P_R$  means average transmit power at R,  $\mathbf{x}_S[\omega] \sim \mathcal{CN}(0, 1)$  represents the intended signal emitted from S,  $\omega \in \{1, 2, \dots, n\}$  denotes the symbol index in a transmission block and  $n$  measures the block-length, i.e., the total number of channel uses in each specific transmission slot.  $\mathbf{x}_R[\omega] = \mathbf{x}_S[\omega - \bar{\omega}]$  is the forwarded version of  $\mathbf{x}_S[\omega - \bar{\omega}]$  after decoding and recoding where  $\mathbf{x}_R[\omega] \sim \mathcal{CN}(0, 1)$ , and integer  $\bar{\omega}$  represents the number of delayed symbols due to signal processing. The AWGNs received at R and D are respectively marked as  $\mathbf{n}_R$  and  $\mathbf{n}_D$ , subjected to  $\mathbf{n}_R[\omega] \sim \mathcal{CN}(0, \sigma_R^2)$  and  $\mathbf{n}_D[\omega] \sim \mathcal{CN}(0, \sigma_D^2)$ . In the FD SWIPT mode, R suffers from the SI which will definitely degrade R's reception quality. Thanks to the promising SIC techniques, R can debilitate the SI up to a relatively low degree. Practically, constrained by computation capacity and impanelment complexity, the perfect SIC cannot be reached. Thus, we consider a practical scenario where imperfect SIC assumption is adopted, and variable  $k \in (0, 1]$  represents the SIC coefficient which implies different SIC levels.

When R does decide to broadcast covert message, the received signals at R and D can be expressed respectively as

$$\mathbf{y}_R[\omega] = \sqrt{P_S}h_{SR}\mathbf{x}_S[\omega] + \sqrt{kP_R}h_{RR}\mathbf{x}_R[\omega] + \sqrt{kP_\Delta}h_{RR}\mathbf{x}_c[\omega] + \mathbf{n}_R[\omega], \quad (4)$$

$$\mathbf{y}_D[\omega] = \sqrt{P_S}h_{SD}\mathbf{x}_S[\omega] + \sqrt{P_R}h_{RD}\mathbf{x}_R[\omega] + \sqrt{P_\Delta}h_{RD}\mathbf{x}_c[\omega] + \mathbf{n}_D[\omega], \quad (5)$$

where  $P_\Delta$  means average transmit power of covert message  $\mathbf{x}_c$  subjected to  $\mathbf{x}_c[\omega] \sim \mathcal{CN}(0, 1)$ . Note that  $P_\Delta$  merely comes from the constant energy supply.

Enabling the FD SWIPT mode, the PS-based EH protocol is adopted in this paper. Specifically, R splits the power of received signal into  $\rho : (1 - \rho)$  proportions. The  $\rho$  portion of the received signal power is used to EH and the remaining  $(1 - \rho)$  portion is allocated to information processing. Therefore, after ignoring the negligible energy harvested from the AWGN, the energy harvested at R in each time slot can be respectively calculated as

$$E_{FS0} = \eta\rho \left( P_s |h_{SR}|^2 + kP_R |h_{RR}|^2 \right), \quad (6)$$

$$E_{FS1} = \eta\rho \left( P_s |h_{SR}|^2 + kP_R |h_{RR}|^2 + kP_\Delta |h_{RR}|^2 \right), \quad (7)$$

where the lower suffix "FS0" refers to the circumstance in which the FD SWIPT mode is invoked without sending covert message, another lower suffix "FS1" means that the FD SWIPT mode with covert message is adopted. Particularly, we constrain the total transmit power at R in the

FD SWIPT mode as  $P_{\text{FS0}} = P_{\text{R}}$  and  $P_{\text{FS1}} = P_{\text{R}} + P_{\Delta}$ , respectively. Hence, (6) and (7) can be reconstructed uniformly as

$$E_{\text{FS}} = \eta\rho \left( P_s |h_{\text{SR}}|^2 + kP_{\text{FS}} |h_{\text{RR}}|^2 \right), \quad (8)$$

where  $P_{\text{FS}} \in \{P_{\text{FS0}}, P_{\text{FS1}}\}$  and  $E_{\text{FS}} \in \{E_{\text{FS0}}, E_{\text{FS1}}\}$ . Note that  $P_{\text{R}} = E_{th}$  holds for each specific transmission block, the lower suffixes “FS”, “FS0” and “FS1” designed in this paper is for concise expression. In any specific mathematical expression, “FS” is applied to solely invoke “FS0” or “FS1”, and no combinations of them will be used. It is worth noting that the harvested energy is collected via the MB at the first place, and then transferred into the PEC within ignorable time duration when the FD SWIPT mode completes.

### III. MARKOV CHAIN AND STATIONARY DISTRIBUTION

Enabling the FD SWIPT mode at R, the hybrid energy container composed of the PEC and the MB is considered in our proposed model. This hybrid energy container system makes R possible to absorb and release energy at the same time, which plays the essential role of hardware foundation in the FD SWIPT mode. However, it leads to highly complex and dynamic charge-discharge behaviors at R, which poses solid obstacle for tracking energy state changes mathematically. To tackle this problem, the energy capacity of PEC is firstly discretized. Then, the MC is invoked to track the complex transmission procedure among discrete energy states. Via the stationary distribution of the MC, the probability of satisfied energy requirement is determined.

#### A. Energy Discretization

To describe the dynamic charging and discharging behaviors of the PEC, we need to discretize the battery capacity into discrete energy states delicately. Each energy state implies the available energy remained in the PEC, which can be reached by calculating the product of the corresponding number of energy levels and the unit energy level. In details, the PEC is quantized into  $L + 1$  levels, and each energy level characterizes an energy unit equal to  $C_{\text{P}}/L$  where  $C_{\text{P}}$  represents the energy capacity of the PEC. Therefore, the  $i$ -th energy state is defined as  $E_i = iC_{\text{P}}/L, i \in \{0, 1, \dots, L\}$ . In the case of infinite energy discretization, i.e.,  $L \rightarrow +\infty$ , the proposed discrete battery model can tightly track the behavior of continuous linear battery which is widely applied in the literature. Note that  $C_{\text{P}} \geq E_{th}$  is considered in this paper, otherwise

R gets no opportunity working in the FD SWIPT mode. It is also worthy to declare that the analysis of energy discretization concentrates on arbitrary transmission block.

In the PEH mode, the discretized amount of energy absorbed by the PEC can be derived as

$$\Xi_{\text{PEH}} \triangleq \left\lfloor \frac{E_{\text{PEH}}}{C_{\text{P}}/L} \right\rfloor \frac{C_{\text{P}}}{L} = \frac{q_{\text{PEH}} C_{\text{P}}}{L}, \quad (9)$$

where  $\lfloor \cdot \rfloor$  denotes the floor function and  $q_{\text{PEH}} \in \{1, 2, \dots, L\}$  is defined for notation concision. Here, without loss of generality, we declare that the  $i$ -th energy state represents the initial energy amount available in the PEC. After charging in the PEH mode, if  $E_i + \Xi_{\text{PEH}} \geq C_{\text{P}}$ , the PEC will be charged to the maximal capacity  $E_L = C_{\text{P}}$  and any overflowed energy has to be abandoned. Otherwise, the latest energy state after charging is  $E_{i+q_{\text{PEH}}} = E_i + \Xi_{\text{PEH}}$  which is guaranteed to be fully accommodated by the PEC.

In the FD SWIPT mode, the harvested energy should be first stored in the MB and then delivered into the PEC when the FD SWIPT mode terminates. Because the MB is subjected to a predefined energy capacity  $C_{\text{M}}$ , the potential amount of energy transferred into the PEC should be reasonably constrained as  $\min\{E_{\text{FS}}, C_{\text{M}}\}$  where the function  $\min\{x, y\}$  outputs the smaller value between  $x$  and  $y$ . practically, energy transfer from the MB to the PEC suffers from circuitry attenuation. Thus, the actual amount of energy absorbed by the PEC can be given by

$$\hat{E}_{\text{FS}} = \eta' \times \min\{E_{\text{FS}}, C_{\text{M}}\}, \quad (10)$$

where  $\eta'$  denotes the energy transfer coefficient from the MB to the PEC, for circuitry attenuation. Furthermore, the discretized amount of energy absorbed by the PEC should be expressed as

$$\Xi_{\text{FS}} \triangleq \left\lfloor \frac{\hat{E}_{\text{FS}}}{C_{\text{P}}/L} \right\rfloor \frac{C_{\text{P}}}{L} = \frac{q_{\text{FS}} C_{\text{P}}}{L}, \quad (11)$$

where  $q_{\text{FS}} \in \{1, 2, \dots, L\}$  is stated for brief expression. While harvesting energy in the FD SWIPT mode, R should decode the source signal and forward the recoded information to D. Invoking the energy requirement, the consumed energy from the PEC should locates at  $E_{\text{FS}}^{\text{C}} \in [E_{\text{th}}, E_i]$  where we set  $E_{\text{FS}}^{\text{C}} = P_{\text{R}} = E_{\text{th}} = 0.6C_{\text{P}}$  for each transmission slot for simplicity. After discretization, the amount of energy consumption at the PEC can be given by

$$\Xi_{\text{FS}}^{\text{C}} = \left\lceil \frac{E_{\text{FS}}^{\text{C}}}{C_{\text{P}}/L} \right\rceil \frac{C_{\text{P}}}{L} = \frac{q_{\text{FS}}^{\text{C}} C_{\text{P}}}{L}, \quad (12)$$

where  $\lceil \cdot \rceil$  stands as the ceiling function, and  $q_{\text{FS}}^{\text{C}}$  is defined for notation simplicity. It is worth noting that R may privately broadcast covert message under the cover of the legitimate forwarded signal. The energy supporting covert communication solely comes from the additional energy

supply unknown by the legitimate party and the transmit power of covert message is fixed as  $P_\Delta$ . Similarly, if  $E_i - \Xi_{\text{FS}}^{\text{C}} + \Xi_{\text{FS}} \geq C_1$ , the PEC will be fully charged to  $E_L = C_P$ . On the contrary, the latest energy state after charging is  $E_{i-q_{\text{FS}}^{\text{C}}+q_{\text{FS}}} = E_i - \Xi_{\text{FS}}^{\text{C}} + \Xi_{\text{FS}}$ .

For clarity, we pose the following statement. At the beginning of the  $(g+1)$ -th block, the initial energy state  $E_i[g+1]$  is merely determined by the transmission mode and energy variation occurred in the adjacently former block, i.e., the  $g$ -th block. Note that  $E_i[g+1]$  is independent to any transmission block before the  $g$ -th block, which implies the Markov property. Specifically,  $E_i[g+1] = \min\{E_i[g] + \Xi_{\text{PEH}}, C_P\}$  and  $E_i[g+1] = \min\{E_i[g] - \Xi_{\text{FS}}^{\text{C}} + \Xi_{\text{FS}}, C_P\}$  correspond respectively to the PEH mode and the FD SWIPT mode applied at R in the  $g$ -th block. Hence, energy state transition among different blocks can be characterized and tracked by the MC. From the aforementioned analysis, we note that energy state transition process in our proposed system is time-independent, thus the MC is considered as homogeneous in time domain.

### B. Markov Chain

Following the energy discretization in a specific transmission block and the transition relationship between energy states for different blocks, we are able to track the transition procedure of energy states at the PEC among multiple transmission blocks as a finite-state time-homogeneous MC. Note that modeling the energy state transition process is indeed not necessary for the MB, because it only plays as a temporary energy storage in the FD SWIPT mode. The transition probability  $p_{i,j}$  denotes the probability of energy state transition from  $E_i$  to  $E_j$ , which is occurred between the beginning of a transmission block and that of the next transmission block. The energy state transitions of the PEC can be stated comprehensively in the following six cases:

1) From  $E_0$  to  $E_0$ : When initial energy at the PEC is empty, it surly cannot afford the FD SWIPT mode. After a transmission block, the residual energy yet remains empty in the considered case. It indicates that the total harvested energy in this PEH block is discretized to zero, namely,  $\Xi_{\text{PEH}} = 0$ . Invoking (1) and (9), the transition probability of states  $E_0 \rightarrow E_0$  can be given by

$$p_{0,0} = \Pr(q_{\text{PEH}} = 0) = \Pr\left(|h_{\text{SR}}|^2 < \frac{C_P}{\eta P_s L}\right). \quad (13)$$

For  $h_{\text{SR}}$  is subjected to Rayleigh fading and  $\mathbb{E}\{|h_{\text{SR}}|^2\} = \Omega_{\text{SR}}$ ,  $|h_{\text{SR}}|^2$  follows the Exponential distribution with mean  $\Omega_{\text{SR}}$ . Thus, the cumulative distribution function (CDF) of  $|h_{\text{SR}}|^2$  can be derived as  $F_{|h_{\text{SR}}|^2}(x) = 1 - \exp(-x/\Omega_{\text{SR}})$ . Furthermore, we get

$$p_{0,0} = F_{|h_{\text{SR}}|^2}\left(\frac{C_P}{\eta P_s L}\right). \quad (14)$$

2) From  $E_L$  to  $E_L$ : In this case, the initial energy certainly satisfies the energy requirement. Thus, whether R works in the PEH mode or the FD SWIPT mode depends merely on the SNR requirement. If the PEH mode is turned on, the harvested energy in this case can be any possible value, since the PEC cannot absorb additional energy any more. If the FD SWIPT mode is activated, the consumed energy should be less than or equal to its harvested counterpart. From (8), (11) and (12), the transition probability of states  $E_L \rightarrow E_L$  can be shown as

$$p_{L,L} = \Pr(\gamma_{SD} \geq \gamma_{th}) + \Pr(\gamma_{SD} < \gamma_{th}) \Pr(\Xi_{FS}^C \leq \Xi_{FS}). \quad (15)$$

Similar to the derivation of (14), we can obtain  $q_{SD} = \Pr(\gamma_{SD} < \gamma_{th}) = F_{|h_{SD}|^2}(\sigma_D^2 \gamma_{th}/P_S)$  and  $\Pr(\gamma_{SD} \geq \gamma_{th}) = 1 - F_{|h_{SD}|^2}(\sigma_D^2 \gamma_{th}/P_S) = 1 - q_{SD}$ . Regarding  $\Pr(\Xi_{FS}^C \leq \Xi_{FS})$ , we obtain

$$\begin{aligned} & \Pr(\Xi_{FS}^C \leq \Xi_{FS}) \\ &= \Pr\left[\left(q_{FS}^C \leq \frac{\eta' E_{FS}}{C_P/L}\right) \cap (E_{FS} < C_M)\right] + \Pr\left[\left(q_{FS}^C \leq \frac{\eta' C_M}{C_P/L}\right) \cap (E_{FS} \geq C_M)\right] \\ &= \begin{cases} \Pr\left(E_{FS} \geq \frac{q_{FS}^C C_P}{\eta' L}\right), & C_M \geq \frac{q_{FS}^C C_P}{\eta' L} \\ 0, & C_M < \frac{q_{FS}^C C_P}{\eta' L} \end{cases}. \end{aligned} \quad (16)$$

Invoking (8), we can gain

$$\Pr\left(E_{FS} \geq \frac{q_{FS}^C C_P}{\eta' L}\right) = \Pr\left(Z \geq \frac{q_{FS}^C C_P}{\eta \rho \eta' L}\right), \quad (17)$$

where  $Z = P_S |h_{SR}|^2 + k P_{FS} |h_{RR}|^2$ . Via convolution of two Exponential distribution variables, we obtain the CDF of  $Z$  as

$$F_Z(x) = \begin{cases} 1 - \frac{P_S \Omega_{SR}}{P_S \Omega_{SR} - k P_{FS} \Omega_{RR}} e^{-\frac{x}{P_S \Omega_{SR}}} + \frac{k P_{FS} \Omega_{RR}}{P_S \Omega_{SR} - k P_{FS} \Omega_{RR}} e^{-\frac{x}{k P_{FS} \Omega_{RR}}}, & P_S \Omega_{SR} \neq k P_{FS} \Omega_{RR} \\ \frac{1}{2} \gamma\left(2, \frac{x}{P_S \Omega_{SR}}\right), & P_S \Omega_{SR} = k P_{FS} \Omega_{RR} \end{cases}, \quad (18)$$

where  $\gamma(\cdot, \cdot)$  is the lower incomplete Gamma function. Furthermore, we get

$$\Pr\left(E_{FS} \geq \frac{q_{FS}^C C_P}{\eta' L}\right) = 1 - F_Z\left(\frac{q_{FS}^C C_P}{\eta \rho \eta' L}\right). \quad (19)$$

Finally, combining (15), (16) and (19), we can obtain

$$p_{L,L} = \begin{cases} 1 - q_{SD} F_Z\left(\frac{q_{FS}^C C_P}{\eta \rho \eta' L}\right), & C_M \geq \frac{q_{FS}^C C_P}{\eta' L} \\ 1 - q_{SD}, & C_M < \frac{q_{FS}^C C_P}{\eta' L} \end{cases}. \quad (20)$$

3) From  $E_i$  to  $E_j$  ( $0 \leq i < j < L$ ): It is easy to find that the energy requirement in this case is not always met. If the initial energy state cannot satisfy the energy requirement, i.e.,  $E_i < E_{th}$ , the PEH mode will be selected. Otherwise, we need to evaluate whether the SNR requirement is met or not. When  $\gamma_{SD} \geq \gamma_{th}$ , R will choose the PEH mode. On the contrary, R will work in the FD SWIPT mode. Thus, the transition probability of states  $E_i \rightarrow E_j$  can be expressed as

$$\begin{aligned}
p_{i,j} &= q_{SD} \Pr(E_i < E_{th}) \Pr(q_{PEH} = j - i) + q_{SD} \Pr(E_i \geq E_{th}) \Pr(q_{FS} - q_{FS}^C = j - i) \\
&\quad + (1 - q_{SD}) \Pr(q_{PEH} = j - i) \\
&= \begin{cases} \Pr(q_{PEH} = j - i), & i < \varphi \\ (1 - q_{SD}) \Pr(q_{PEH} = j - i) + q_{SD} \Pr(q_{FS} - q_{FS}^C = j - i), & i \geq \varphi \end{cases}, \quad (21)
\end{aligned}$$

where  $\varphi = \left\lceil \frac{E_{th}}{C_P/L} \right\rceil$  denotes the total number of energy units needed to represent the energy requirement in the discretized energy regime.

Next, we calculate  $\Pr(q_{PEH} = j - i)$  and  $\Pr(q_{FS} - q_{FS}^C = j - i)$ , shown respectively as (22) and (23) in the following.

$$\begin{aligned}
\Pr(q_{PEH} = j - i) &= \Pr\left(\frac{(j-i)C_P}{\eta P_S L} \leq |h_{SR}|^2 < \frac{(j-i+1)C_P}{\eta P_S L}\right) \\
&= F_{|h_{SR}|^2}\left(\frac{(j-i+1)C_P}{\eta P_S L}\right) - F_{|h_{SR}|^2}\left(\frac{(j-i)C_P}{\eta P_S L}\right). \quad (22)
\end{aligned}$$

$$\begin{aligned}
&\Pr(q_{FS} - q_{FS}^C = j - i) \\
&= \begin{cases} 0, & C_M < \frac{(j-i+q_{FS}^C)C_P}{\eta' L} \\ 1 - F_Z\left(\frac{(j-i+q_{FS}^C)C_P}{\eta \rho \eta' L}\right), & \frac{(j-i+q_{FS}^C)C_P}{\eta' L} \leq C_M < \frac{(j-i+q_{FS}^C+1)C_P}{\eta' L} \\ F_Z\left(\frac{(j-i+q_{FS}^C+1)C_P}{\eta \rho \eta' L}\right) - F_Z\left(\frac{(j-i+q_{FS}^C)C_P}{\eta \rho \eta' L}\right), & C_M \geq \frac{(j-i+q_{FS}^C+1)C_P}{\eta' L} \end{cases}. \quad (23)
\end{aligned}$$

Combining (21), (22) and (23), we get the probability of transition  $E_i \rightarrow E_j$  as

$$p_{i,j} = \begin{cases} F_{|h_{SR}|^2}\left(\frac{(j-i+1)C_P}{\eta P_S L}\right) - F_{|h_{SR}|^2}\left(\frac{(j-i)C_P}{\eta P_S L}\right), & i < \varphi \\ (1 - q_{SD}) \\ \quad \times \left[ F_{|h_{SR}|^2}\left(\frac{(j-i+1)C_P}{\eta P_S L}\right) - F_{|h_{SR}|^2}\left(\frac{(j-i)C_P}{\eta P_S L}\right) \right], & i \geq \varphi \& C_M < \frac{(j-i+q_{FS}^C)C_P}{\eta' L} \\ (1 - q_{SD}) \\ \quad \times \left[ F_{|h_{SR}|^2}\left(\frac{(j-i+1)C_P}{\eta P_S L}\right) - F_{|h_{SR}|^2}\left(\frac{(j-i)C_P}{\eta P_S L}\right) \right] \\ \quad + q_{SD} \left[ 1 - F_Z\left(\frac{(j-i+q_{FS}^C)C_P}{\eta \rho \eta' L}\right) \right], & i \geq \varphi \& \frac{(j-i+q_{FS}^C)C_P}{\eta' L} \\ \quad \leq C_M < \frac{(j-i+q_{FS}^C+1)C_P}{\eta' L} \\ (1 - q_{SD}) \\ \quad \times \left[ F_{|h_{SR}|^2}\left(\frac{(j-i+1)C_P}{\eta P_S L}\right) - F_{|h_{SR}|^2}\left(\frac{(j-i)C_P}{\eta P_S L}\right) \right] \\ \quad + q_{SD} \\ \quad \times \left[ F_Z\left(\frac{(j-i+q_{FS}^C+1)C_P}{\eta \rho \eta' L}\right) - F_Z\left(\frac{(j-i+q_{FS}^C)C_P}{\eta \rho \eta' L}\right) \right], & i \geq \varphi \& C_M \geq \frac{(j-i+q_{FS}^C+1)C_P}{\eta' L} \end{cases}. \quad (24)$$



4) From  $E_i$  to  $E_i$  ( $0 < i < L$ ): In this case, it is not certain whether the energy requirement is met or not. If  $E_i < E_{th}$ , the PEH mode will be invoked and the harvested energy should be discretized as zero. If  $E_i \geq E_{th}$  and  $\gamma_{SD} \geq \gamma_{th}$ , the PEH mode is enabled and the harvested energy should also be discretized as zero, too. If  $E_i \geq E_{th}$  and  $\gamma_{SD} < \gamma_{th}$ , the FD SWIPT mode will be selected, the discretized amount of consumed energy should be equal to that of harvested energy. Hence, the transition probability of states  $E_i \rightarrow E_i$  can be calculated as

$$\begin{aligned} p_{i,i} &= (1 - q_{SD}) \Pr(q_{PEH} = 0) \\ &\quad + q_{SD} \Pr(E_i < E_{th}) \Pr(q_{PEH} = 0) + q_{SD} \Pr(E_i \geq E_{th}) \Pr(q_{FS} - q_{FS}^C = 0) \\ &= \begin{cases} \Pr(q_{PEH} = 0), & i < \varphi \\ (1 - q_{SD}) \Pr(q_{PEH} = 0) + q_{SD} \Pr(q_{FS} - q_{FS}^C = 0), & i \geq \varphi \end{cases}, \end{aligned} \quad (25)$$

where  $\Pr(q_{PEH} = 0)$  and  $\Pr(q_{FS} - q_{FS}^C = 0)$  are given respectively by (14) and (26) shown as

$$\begin{aligned} \Pr(q_{FS} - q_{FS}^C = 0) &= \Pr(q_{FS} = q_{FS}^C) \\ &= \begin{cases} 0, & C_M < \frac{q_{FS}^C C_P}{\eta' L} \\ 1 - F_Z\left(\frac{q_{FS}^C C_P}{\eta \rho \eta' L}\right), & \frac{q_{FS}^C C_P}{\eta' L} \leq C_M < \frac{(q_{FS}^C + 1) C_P}{\eta' L} \\ F_Z\left(\frac{(q_{FS}^C + 1) C_P}{\eta \rho \eta' L}\right) - F_Z\left(\frac{q_{FS}^C C_P}{\eta \rho \eta' L}\right), & C_M \geq \frac{(q_{FS}^C + 1) C_P}{\eta' L} \end{cases}. \end{aligned} \quad (26)$$

Substituting (14) and (26) into (25), we get the transition probability of states  $E_i \rightarrow E_i$  as

$$p_{i,i} = \begin{cases} F_{|h_{SR}|^2}\left(\frac{C_P}{\eta P_S L}\right), & i < \varphi \\ (1 - q_{SD}) F_{|h_{SR}|^2}\left(\frac{C_P}{\eta P_S L}\right), & i \geq \varphi \& C_M < \frac{q_{FS}^C C_P}{\eta' L} \\ (1 - q_{SD}) F_{|h_{SR}|^2}\left(\frac{C_P}{\eta P_S L}\right) \\ + q_{SD} \left[ 1 - F_Z\left(\frac{q_{FS}^C C_P}{\eta \rho \eta' L}\right) \right], & i \geq \varphi \& \frac{q_{FS}^C C_P}{\eta' L} \leq C_M < \frac{(q_{FS}^C + 1) C_P}{\eta' L} \\ (1 - q_{SD}) F_{|h_{SR}|^2}\left(\frac{C_P}{\eta P_S L}\right) \\ + q_{SD} \left[ F_Z\left(\frac{(q_{FS}^C + 1) C_P}{\eta \rho \eta' L}\right) - F_Z\left(\frac{q_{FS}^C C_P}{\eta \rho \eta' L}\right) \right], & i \geq \varphi \& C_M \geq \frac{(q_{FS}^C + 1) C_P}{\eta' L} \end{cases}. \quad (27)$$

5) From  $E_i$  to  $E_j$  ( $0 \leq j < i \leq L$ ): Obviously, this circumstance can only occur in the FD SWIPT mode because the PEH mode can exclusively lead to energy increasing or energy unchanged. Therefore, the transition probability of states  $E_i \rightarrow E_j$  can be derived as

$$\begin{aligned} p_{i,j} &= \Pr(\gamma_{SD} < \gamma_{th}) \Pr(E_i \geq E_{th}) \Pr(q_{FS}^C - q_{FS} = i - j) \\ &= \begin{cases} 0, & i < \varphi \\ q_{SD} \Pr(q_{FS}^C - q_{FS} = i - j), & i \geq \varphi \end{cases}. \end{aligned} \quad (28)$$

Next, we need to calculate  $\Pr(q_{\text{FS}}^{\text{C}} - q_{\text{FS}} = i - j)$ , shown as

$$\Pr(q_{\text{FS}}^{\text{C}} - q_{\text{FS}} = i - j) = \begin{cases} 0, & C_{\text{M}} < \frac{[q_{\text{FS}}^{\text{C}} - (i-j)]C_{\text{P}}}{\eta' L} \\ 1 - F_Z\left(\frac{[q_{\text{FS}}^{\text{C}} - (i-j)]C_{\text{P}}}{\eta\rho\eta' L}\right), & \frac{[q_{\text{FS}}^{\text{C}} - (i-j)]C_{\text{P}}}{\eta' L} \leq C_{\text{M}} < \frac{[q_{\text{FS}}^{\text{C}} - (i-j)+1]C_{\text{P}}}{\eta' L} \\ F_Z\left(\frac{[q_{\text{FS}}^{\text{C}} - (i-j)+1]C_{\text{P}}}{\eta\rho\eta' L}\right) - F_Z\left(\frac{[q_{\text{FS}}^{\text{C}} - (i-j)]C_{\text{P}}}{\eta\rho\eta' L}\right), & C_{\text{M}} \geq \frac{[q_{\text{FS}}^{\text{C}} - (i-j)+1]C_{\text{P}}}{\eta' L} \end{cases} \quad (29)$$

Invoking (28) and (29), we can express the transition probability of state  $E_i \rightarrow E_j$  as

$$p_{i,j} = \begin{cases} 0, & i < \varphi \parallel \left(j \geq \varphi \& C_{\text{M}} < \frac{[q_{\text{FS}}^{\text{C}} - (i-j)]C_{\text{P}}}{\eta' L}\right) \\ q_{\text{SD}} \left(1 - F_Z\left(\frac{[q_{\text{FS}}^{\text{C}} - (i-j)]C_{\text{P}}}{\eta\rho\eta' L}\right)\right), & i \geq \varphi \& \frac{[q_{\text{FS}}^{\text{C}} - (i-j)]C_{\text{P}}}{\eta' L} \leq C_{\text{M}} < \frac{[q_{\text{FS}}^{\text{C}} - (i-j)+1]C_{\text{P}}}{\eta' L} \\ q_{\text{SD}} \left[F_Z\left(\frac{[q_{\text{FS}}^{\text{C}} - (i-j)+1]C_{\text{P}}}{\eta\rho\eta' L}\right) - F_Z\left(\frac{[q_{\text{FS}}^{\text{C}} - (i-j)]C_{\text{P}}}{\eta\rho\eta' L}\right)\right], & i \geq \varphi \& C_{\text{M}} \geq \frac{[q_{\text{FS}}^{\text{C}} - (i-j)+1]C_{\text{P}}}{\eta' L} \end{cases} \quad (30)$$

6) From  $E_i$  to  $E_L$  ( $0 \leq i < L$ ): In this circumstance, we cannot make sure what mode is applied by R, for whether the initial energy state can satisfy the energy requirement is not determined. When  $E_i < E_{th}$ , certainly the PEH mode will be activated, and the harvested energy should meet  $\Xi_{\text{PEH}} \geq E_L - E_i$ . Otherwise, if  $\gamma_{\text{SD}} \geq \gamma_{th}$ , the PEH also will be invoked and the harvested energy is supposed to satisfy  $\Xi_{\text{PEH}} \geq E_L - E_i$ . If  $E_i \geq E_{th}$  and  $\gamma_{\text{SD}} < \gamma_{th}$ , the FD SWIPT mode will be selected and the relationship between the harvested energy and the released energy should meet  $\Xi_{\text{PEH}} - \Xi_{\text{PEH}}^{\text{C}} \geq E_L - E_i$ . Thus, the transition probability of states  $E_i \rightarrow E_L$  can be expressed as

$$\begin{aligned} p_{i,L} &= \Pr(\gamma_{\text{SD}} \geq \gamma_{th}) \Pr(q_{\text{PEH}} \geq L - i) + \Pr(\gamma_{\text{SD}} < \gamma_{th}) \Pr(E_i < E_{th}) \Pr(q_{\text{PEH}} \geq L - i) \\ &\quad + \Pr(\gamma_{\text{SD}} < \gamma_{th}) \Pr(E_i \geq E_{th}) \Pr(q_{\text{FS}} - q_{\text{FS}}^{\text{C}} \geq L - i) \\ &= \begin{cases} \Pr(q_{\text{PEH}} \geq L - i), & i < \varphi \\ (1 - q_{\text{SD}}) \Pr(q_{\text{PEH}} \geq L - i) + q_{\text{SD}} \Pr(q_{\text{FS}} - q_{\text{FS}}^{\text{C}} \geq L - i), & i \geq \varphi \end{cases} \end{aligned} \quad (31)$$

Next,  $\Pr(q_{\text{PEH}} \geq L - i)$  and  $\Pr(q_{\text{FS}} - q_{\text{FS}}^{\text{C}} \geq L - i)$  can be derived respectively as

$$\Pr(q_{\text{PEH}} \geq L - i) = 1 - F_{|h_{\text{SR}}|^2}\left(\frac{(L-i)C_{\text{P}}}{\eta P_{\text{S}} L}\right), \quad (32)$$

$$\Pr(q_{\text{FS}} - q_{\text{FS}}^{\text{C}} \geq L - i) = \begin{cases} 0, & C_{\text{M}} < \frac{(L-i+q_{\text{FS}}^{\text{C}})C_{\text{P}}}{\eta' L} \\ 1 - F_Z\left(\frac{(L-i+q_{\text{FS}}^{\text{C}})C_{\text{P}}}{\eta\rho\eta' L}\right), & C_{\text{M}} \geq \frac{(L-i+q_{\text{FS}}^{\text{C}})C_{\text{P}}}{\eta' L} \end{cases} \quad (33)$$



Figure 1. The state transition diagram and the corresponding transition probability matrix of the Markov chain, in the case of  $L = 2$ .

Invoking (31), (32) and (33), we get the transition probability of states  $E_i \rightarrow E_L$ , shown as

$$p_{i,L} = \begin{cases} 1 - F_{|h_{SR}|^2} \left( \frac{(L-i)C_P}{\eta P_S L} \right), & i < \varphi \\ (1 - q_{SD}) \left[ 1 - F_{|h_{SR}|^2} \left( \frac{(L-i)C_P}{\eta P_S L} \right) \right], & i \geq \varphi \& C_M < \frac{(L-i+q_{FS}^C)C_P}{\eta' L} \\ (1 - q_{SD}) \left[ 1 - F_{|h_{SR}|^2} \left( \frac{(L-i)C_P}{\eta P_S L} \right) \right] \\ + q_{SD} \left[ 1 - F_Z \left( \frac{(L-i+q_{FS}^C)C_P}{\eta \rho \eta' L} \right) \right], & i \geq \varphi \& C_M \geq \frac{(L-i+q_{FS}^C)C_P}{\eta' L} \end{cases}. \quad (34)$$

### C. Stationary Distribution

We define  $\mathbf{M} \triangleq \{p_{i,j}\}$  to denote the  $(L+1) \times (L+1)$  state transition matrix. For the convenience of illustration, we provide an example of the possible energy states and the transitions among them in the case of  $L = 2$ . As shown in Figure 1, the state transition diagram and the corresponding transition probability matrix of the MC are clearly depicted.

**Theorem 1:** In this theorem, we derive the probability that the energy status of arbitrary transmission slot meets the given energy condition. With the help of stationary distribution  $\xi$ , for arbitrary transmission slot, we have

$$\Pr(E_i \geq E_{th}) = \sum_{i=\varphi}^L \xi_i, \quad (35)$$

where  $\xi_i \in \xi = (\xi_0, \xi_1, \dots, \xi_L)^T$ , which can be gained by applying method in the following proof.

Furthermore, we can conclude that

$$\Pr(E_i < E_{th}) = 1 - \sum_{i=\varphi}^L \xi_i = \sum_{i=0}^{\varphi-1} \xi_i. \quad (36)$$

*Proof:* Using the similar methods in [29], we can easily verify that the transition matrix  $\mathbf{M}$  is irreducible<sup>1</sup> and row stochastic<sup>2</sup>, which can be verified via Figure 1 as an example. Thus, the stationary distribution  $\boldsymbol{\xi}$  must satisfy the following equation

$$\boldsymbol{\xi} = (\xi_0, \xi_1, \dots, \xi_L)^T = \mathbf{M}^T \boldsymbol{\xi}. \quad (37)$$

By solving the above equation,  $\boldsymbol{\xi}$  can be derived as

$$\boldsymbol{\xi} = (\mathbf{M}^T - \mathbf{I} + \mathbf{B})^{-1} \mathbf{b}, \quad (38)$$

where  $\mathbf{B}_{i,j} = 1, \forall i, j$ ,  $\mathbf{b} = (1, 1, \dots, 1)^T$  and  $\mathbf{I}$  denotes the unit matrix. ■

**Remark 1:** In *Theorem 1*,  $\xi_i$  where  $i \in \{0, 1, \dots, L\}$  represents the stationary probability of the  $i$ -th energy state, on a long-term perspective. The reason why the result  $\Pr(E_i \geq E_{th}) = \sum_{i=\varphi}^L \xi_i$  in *Theorem 1* holds can be straightly explained as that  $\xi_i$  where  $i \geq \varphi$  describes the probability of an arbitrary event whose residual energy is higher than the energy threshold and the probability summation of all these events makes up the overall probability of  $E_i \geq E_{th}$ . It is worth noting that *Theorem 1* serves as the prerequisite for deriving closed-form expressions of transmission outage probability which will be shown in Section V.

#### D. Verification and Discussion

In Figure 2, we illustrate the dynamic charge-discharge behavior of the PEC (subfigure (I)) and the comparison of the steady state distribution gained from the analytical framework in this section against those generated through Monte Carlo simulation (subfigure (II)). Note that for subfigure (I), (II) and (III),  $L = 25$ , for subfigure (IV),  $L = 5$  the other system parameters are all the same among subfigures in Figure 2. The detailed system parameter setups in this figure is in line with that in Section VI.

**Remark 2:** The initial energy remained in the PEC is set to be empty, and as the proposed HOR system runs with respect to (w.r.t.) block numbers, the complex energy accumulation and consumption process can be clearly traced as shown in subfigure (I). Observing subfigure (II),

<sup>1</sup>In a MC, the transition matrix is said to be irreducible if it is possible to reach any other state from any state in finite number of steps. In our MC analysis, all possible energy states communicate so that the transition matrix  $\mathbf{M}$  is irreducible in this paper.

<sup>2</sup>In a MC, the transition matrix is said to be row stochastic if the sum of all the elements in a row is one and all elements are non-negative. In our MC analysis, the transition probabilities from any energy state to all possible energy states sums up to one and the transition probabilities are definitely non-negative, so we say the transition matrix  $\mathbf{M}$  is row stochastic in this paper. We also note that  $\mathbf{M}$  is asymmetric because  $p_{i,j} \neq p_{j,i}, \forall i, j$ , given the aforementioned analysis.

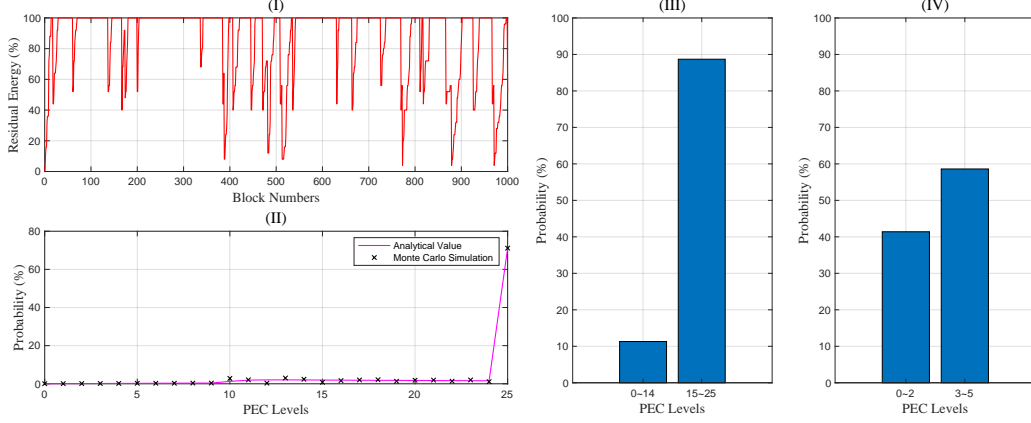


Figure 2. Illustration of residual energy fluctuations, validation of the proposed MC analysis and the impact of energy discretisation levels.

it is confirmed that the proposed analytical model matches the actual distribution very well, validating the effectiveness of analysis on the MC in this section.

**Remark 3:** Comparing subfigures (III) and (IV), one can find that the larger  $L$  (i.e. the PEC levels) is, more likely the residual energy in the PEC can satisfy the “energy requirement” which is hereby quantified as that the residual energy in the PEC is greater than or equal to 60% of the PEC’s capacity. This is reasonable for a two-fold reason: 1) the floor function (e.g., formulas (9) and (11)) used to quantify the discretized amount of energy absorbed by the PEC limits that the proposed energy discretization model has to abandon the overflow energy assimilated; 2) the ceil function (e.g., formula (12)) applied to quantify the discretized amount of energy consumed by the PEC restricts that the proposed energy discretization model should quantify the underflow amount of discretized energy used up by the PEC as an specific integer, which means the proposed model consumes extra energy than its actual counterpart. According to the aforementioned analysis, we can conclude that the larger  $L$  is, i.e., the finer the PEC is mathematically discretized, the more efficiently manipulating of RF energy can reach. A subsequent influence of  $L$  on wireless transmission performance can be found in details in Section VI. However, there exists the inherent trade-off between the computation complexity and energy manipulating efficiency of the proposed energy discretization model so that the value of  $L$  should be chosen carefully and delicately in the practical application scenarios.

Based on the MC analysis, we can mathematically track wireless transmission performance of the proposed HOR protocol, like, the connection outage probability, which will be clearly stated and analyzed in Section V. Besides, the inherent SNR requirement when the FD SWIPT

is invoked restricts that  $\gamma_{SD}$  has to be less  $\gamma_{th}$ , which puts congenital influences on the covert performance analysis in Section IV.

#### IV. COVERT COMMUNICATION PERFORMANCE ANALYSIS

In Section III, we investigated the stationary distribution of energy states discretized at R's PEC, via energy discretization and finite-state homogeneous MC. In this section, we will analyze the covert performance of the proposed HOR protocol. Note that R only intends to broadcast covert message in the case of working in the FD SWIPT mode, because there exists no solid cover in the PEH mode so that D which also plays the role as *warden* can detect the arising of covert communication easily. Thus, this paper focuses on the circumstance in which D performs detection regarding covert communication only in the case of FD SWIPT mode. In the PEH mode, R will not broadcast covert message and D ceases the detection. This consideration is reasonable because the exact work mode R applies is an open consensus among all nodes at the beginning of each specific transmission block. Note that in this section, the constraint  $\gamma_{SD} < \gamma_{th}$  holds due to the nature of the FD SWIPT mode.

##### A. Channel Uncertainty Model

To investigate the impact of channel uncertainty on covert detection performance at D, it is assumed that D gets an imperfect estimation of the wireless channel R→D and the imperfect channel estimation model of D is formulated as

$$h_{RD} = \hat{h}_{RD} + \tilde{h}_{RD}, \quad (39)$$

where  $\hat{h}_{RD} \sim \mathcal{CN}(0, (1 - \beta) \Omega_{RD})$  and  $\tilde{h}_{RD} \sim \mathcal{CN}(0, \beta \Omega_{RD})$  are independent complex Gaussian random variables (RVs) which represent D's channel estimation and the corresponding estimation error, respectively. It is worth noting that  $\beta \in (0, 1)$  measures the degree of channel uncertainty and the aforementioned assumption of Gaussian estimation error comes from the minimum mean square error (MMSE) estimation method. Although the instantaneous knowledge of  $h_{RD}$  that D gains is incomplete and contains estimation error, we assume that D does know the fading distribution to which  $h_{RD}$  is subjected.

##### B. Binary Detection at the Destination

The source node S transmits wireless energy to charge R for gaining assistance helping the main wireless transmission between S and D. As one part of the main party, D performs detection

regarding whether R emits illegitimate information, i.e., covert message, under the cover of legal forwarded version of source messages. Hence, apart from receiving desired information from S and R, D also needs to perform simple (binary) hypothesis test in which  $\mathcal{H}_0$  means the null hypothesis indicating that R does not transmit covert information while  $\mathcal{H}_1$  represents the alternative hypothesis implicating that R does emit the covert message. In a specific transmission slot, we define the False Alarm (i.e., type I error) probability by  $\mathbb{P}_{\text{FA}} \triangleq \Pr(\mathcal{D}_1|\mathcal{H}_0)$  and the Missed Detection (i.e., type II error) probability by  $\mathbb{P}_{\text{MD}} \triangleq \Pr(\mathcal{D}_0|\mathcal{H}_1)$ , where  $\mathcal{D}_1$  and  $\mathcal{D}_0$  represent the binary decisions in favor of the occurrence of covert transmission or not, respectively. Besides, the *a priori* probabilities of hypotheses  $\mathcal{H}_0$  and  $\mathcal{H}_1$  are assumed to be equal (i.e., both are 0.5) in this paper<sup>3</sup>, which is a widely adopted assumption in the field of covert communication. Following this assumption, the detection performance of D is measured by the detection error probability  $\mathbb{P}_{\text{E}}$ , defined as

$$\mathbb{P}_{\text{E}} \triangleq \mathbb{P}_{\text{FA}} + \mathbb{P}_{\text{MD}}. \quad (40)$$

For arbitrary  $\epsilon > 0$ , we define R achieving covert communication if any communication scheme exists satisfying  $\mathbb{P}_{\text{E}} \geq 1 - \epsilon$ . Note that the lower bound on  $\mathbb{P}_{\text{E}}$  characterizes the necessary trade-off between the false alarms and missed detections in a simple hypothesis test. Specifically,  $\mathbb{P}_{\text{E}} \geq 1 - \epsilon$  represents the covert communication constraint and  $\epsilon$  signifies the covert requirement, cause a sufficiently small  $\epsilon$  renders any detector employed at D to be ineffective.

### C. Derivation and Analytics

When a transmission block is determined to adopt the FD SWIPT mode, D would like to keep an eye on whether R broadcasts covert message under the cover of the forwarded version of source information. In the case of FD SWIPT mode, the received signals at D in the  $\omega$ -th channel use within a transmission block can be expressed as

$$\mathbf{y}_{\text{D}}[\omega] = \begin{cases} \sqrt{P_{\text{S}}}h_{\text{SD}}\mathbf{x}_{\text{S}}[\omega] + \sqrt{P_{\text{R}}}h_{\text{RD}}\mathbf{x}_{\text{R}}[\omega] + \mathbf{n}_{\text{D}}[\omega], & \mathcal{H}_0 \\ \sqrt{P_{\text{S}}}h_{\text{SD}}\mathbf{x}_{\text{S}}[\omega] + \sqrt{P_{\text{R}}}h_{\text{RD}}\mathbf{x}_{\text{R}}[\omega] + \sqrt{P_{\Delta}}h_{\text{RD}}\mathbf{x}_{\text{c}}[\omega] + \mathbf{n}_{\text{D}}[\omega], & \mathcal{H}_1 \end{cases}. \quad (41)$$

**Lemma 1:** A radiometer is utilized by D to perform the detection test monitoring potential covert communications launched by R. In the case of availability of noise power at D, it is approved that radiometer is the optimal detector for covert communication detection.

<sup>3</sup>Note that the equal *a priori* probability assumption corresponds to the circumstance in which D has no *a priori* knowledge on whether R emits covert message or not and completely ignores R's covert transmission possibility.

*Proof:* See Appendix A. ■

Applying a radiometer as the optimal detection strategy at D, closed-form expressions of false alarm, missed detection and detection error probabilities for any given threshold  $\tau$  will be derived in the following Theorem. Then, closed-form expressions of the optimal detection threshold  $\tau$  and minimum detection error probability will be derived and given. The impacts of imperfect channel estimation on minimum detection error probability will be analyzed via discussion of its monotonicity w.r.t.  $\beta$ .

**Theorem 2:** For arbitrary threshold  $\tau$ , closed-form expressions of false alarm and missed detection probabilities can be respectively given by

$$\mathbb{P}_{\text{FA}} = \begin{cases} \exp\left(\frac{j_0 - \tau}{\beta P_R \Omega_{\text{RD}}}\right), & \tau \geq j_0 \\ 1, & \text{otherwise} \end{cases}, \quad (42)$$

$$\mathbb{P}_{\text{MD}} = \begin{cases} 1 - \exp\left(\frac{j_1 - \tau}{\beta(P_R + P_\Delta)\Omega_{\text{RD}}}\right), & \tau \geq j_1 \\ 0, & \text{otherwise} \end{cases}, \quad (43)$$

where  $j_0 = P_S |h_{\text{SD}}|^2 + P_R |\hat{h}_{\text{RD}}|^2 + \sigma_D^2$  and  $j_1 = P_S |h_{\text{SD}}|^2 + (P_R + P_\Delta) |\hat{h}_{\text{RD}}|^2 + \sigma_D^2$ . Furthermore, invoking (40), (42) and (43), we can derive closed-form expression of the detection error probability, shown as

$$\mathbb{P}_{\text{E}} = \begin{cases} 1, & \tau < j_0 \\ \exp\left(\frac{j_0 - \tau}{\beta P_R \Omega_{\text{RD}}}\right), & j_0 \leq \tau < j_1 \\ 1 + \exp\left(\frac{j_0 - \tau}{\beta P_R \Omega_{\text{RD}}}\right) - \exp\left(\frac{j_1 - \tau}{\beta(P_R + P_\Delta)\Omega_{\text{RD}}}\right), & \tau \geq j_1 \end{cases}. \quad (44)$$

*Proof:* See Appendix B. ■

**Theorem 3:** The optimal detection threshold of D's radiometer, which is supposed to minimize  $\mathbb{P}_{\text{E}}$ , is given by

$$\tau^* = \begin{cases} j_1, & j_1 \geq \tau_{k_1=0} \\ \tau_{k_1=0}, & j_1 < \tau_{k_1=0} \end{cases}, \quad (45)$$

where

$$\tau_{k_1=0} = -\frac{\beta P_R (P_R + P_\Delta) \Omega_{\text{RD}}}{P_\Delta} \ln \frac{P_R}{P_R + P_\Delta} + P_S |h_{\text{SD}}|^2 + \sigma_D^2. \quad (46)$$

*Proof:* See Appendix C. ■



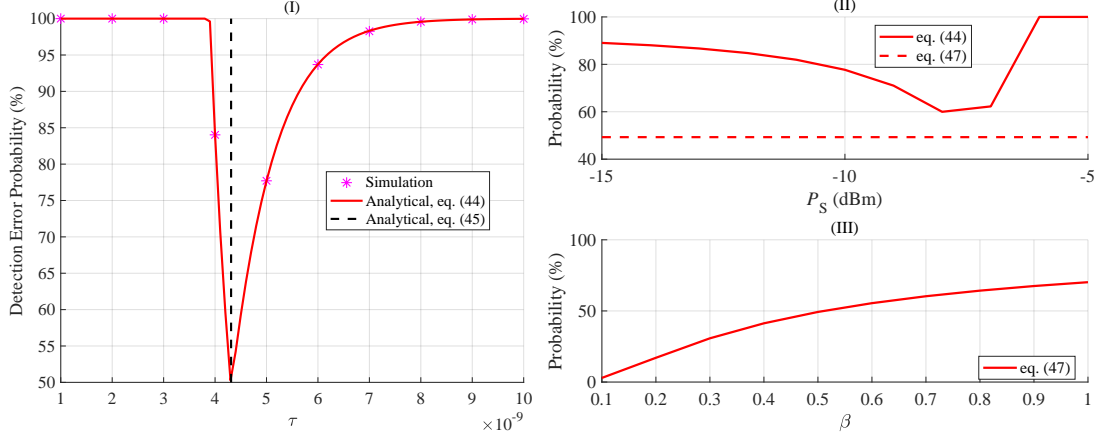


Figure 3. Validation of the derived closed-form expressions of detection error probability and the optimal detection threshold, illustration of performance superiority of the proposed minimum detection error probability and its monotonicity w.r.t.  $\beta$ .

**Corollary 1:** To achieve the best detection performance, D will always select the optimal detection threshold as per (45). Thus, closed-form expression of minimum detection error probability can be calculated as

$$\mathbb{P}_E^* = \begin{cases} \exp\left(\frac{j_0 - j_1}{\beta P_R \Omega_{RD}}\right), & j_1 \geq \tau_{k1=0} \\ 1 + \exp\left(\frac{j_0 - \tau_{k1=0}}{\beta P_R \Omega_{RD}}\right) - \exp\left(\frac{j_1 - \tau_{k1=0}}{\beta (P_R + P_\Delta) \Omega_{RD}}\right), & j_1 < \tau_{k1=0} \end{cases}. \quad (47)$$

**Remark 4:** According to **Theorem 2**, **Theorem 3** and **Corollary 1**, it is confirmed that  $\mathbb{P}_E$ ,  $\tau^*$  and  $\mathbb{P}_E^*$  are independent to parameters  $k$ ,  $L$ ,  $\gamma_{th}$ ,  $C_M$ ,  $\eta$ ,  $\eta'$ ,  $\sigma_R^2$ ,  $h_{RR}$  and  $h_{SR}$ . This is because, concisely speaking, covert communication is constrained to be possible only within the FD SWIPT mode, and parameters  $C_P$  and  $E_{th}$  can affect covert metrics in the manner of the aforementioned  $P_R = E_{th} = 0.6C_P$ . Moreover,  $\mathbb{P}_E^*$  is not subjected to  $P_S$  and  $h_{SD}$  either, because of subtractions of  $j_0 - j_1$ ,  $j_0 - \tau_{k1=0}$  and  $j_1 - \tau_{k1=0}$ . This finding can guide designers to understand clearly what parameters are valid to pose impacts on covert communication detection performance.

With the help of **Corollary 1**, it is mathematically guaranteed that the detection error probability at D is minimized on the perspective of imperfect channel estimation. However, how does the factor  $\beta$  influence the performance of minimum detection error probability? This question motivates us to provide the following Corollary.

**Corollary 2:** Minimum detection error probability  $\mathbb{P}_E^*$  is monotonically increasing function w.r.t.  $\beta$ .

*Proof:* See Appendix D. ■

**Remark 5:** Based on *Corollary 2*, the imperfect channel estimation is proved to be an important factor posing significant impacts on  $\mathbb{P}_E^*$ . A smaller  $\beta$ , i.e., the better channel estimation method, is desired to enhance the covert communication detection performance at D.

To better show the covert communication performance analysis and verify the correctness of the corresponding analytical expressions, Figure 3 is illustrated in which  $\beta = 0.5$  stands unless otherwise specified and the other system parameters are set in line with those in Section VI. Note that in Figure 3, we evaluate covert metrics for arbitrarily selected transmission block pair in which  $h_{SD} = -0.0010 - 0.0027j$  and  $h_{RD} = 0.0261 + 0.0526j$  stand. From subfigure (I), the Monte Carlo simulation nodes match perfectly with the analytical curve of (44) and the dash line generated from (45) coincides tightly with the simulated optimal  $\tau$ 's coordinate, validating the correctness of the derived analytical expressions in *Theorem 2*, *Theorem 3*. Subfigure (II) depicts clearly that applying *Corollary 1* can significantly reduce the detection error probability, compared with its counterpart without the optimal detection threshold. It can also be observed from subfigure (II) that the curve of  $\mathbb{P}_E^*$  holds instant w.r.t.  $P_S$ , the reason was explained in *Remark 4*. Last but not least, subfigure (III) shows that  $\mathbb{P}_E^*$  is a monotonically increasing function w.r.t.  $\beta$ , justifying the effectiveness of *Corollary 2* and *Remark 5*.

In this section, we analyzed the covert communication performance by proving the optimality of radiometer on detection of potential covert communication and deriving closed-form expressions of detection error probability. Based on the mathematical analysis, we calculated and stated closed-form expressions of the optimal detection threshold and minimum detection error probability. Note that in this section, we focused on the situation where the FD SWIPT mode is invoked at R. For each particular transmission block which is located in the domain of FD SWIPT, we provided closed-form expressions of the optimal detection threshold and minimum detection probability from the perspective of imperfect channel estimation of instantaneous wireless channel between S and D, which means the values of (45) and (47) stand for this specific transmission block and vary among different transmission blocks when the FD SWIPT mode is activated. Besides, we would like to emphasize hereby that the optimality of our analysis in this section is valid for any particular wireless channel applications when the FD SWIPT mode is active. It is also worth noting that the proposed HOR model inherently limits  $\gamma_{SD} < \gamma_{th}$  for the analysis in this section, due to the SNR requirement.

## V. TRANSMISSION OUTAGE PERFORMANCE ANALYSIS

In this section, a typical transmission performance metrics, namely, transmission outage probability (TOP) is derived and analyzed in details. In this paper, we consider the circumstance in which D applies Maximum Ratio Combination (MRC) protocol to combine the received signals from S and R, when the FD SWIPT mode stands.

In the FD SWIPT mode, invoking (3) and (5), the received SINR at D can be given by

$$\gamma_D = \begin{cases} \gamma_{SD} + Y_{\mathcal{H}_0}, & \mathcal{H}_0 \\ \gamma_{SD} + Y_{\mathcal{H}_1}, & \mathcal{H}_1 \end{cases}, \quad (48)$$

where

$$Y_{\mathcal{H}_0} = \min \left\{ \frac{(1-\rho) P_S |h_{SR}|^2}{(1-\rho) k P_R |h_{RR}|^2 + \sigma_R^2}, \frac{P_R |h_{RD}|^2}{\sigma_D^2} \right\}, \quad (49)$$

$$Y_{\mathcal{H}_1} = \min \left\{ \frac{(1-\rho) P_S |h_{SR}|^2}{(1-\rho) k (P_R + P_\Delta) |h_{RR}|^2 + \sigma_R^2}, \frac{P_R |h_{RD}|^2}{P_\Delta |h_{RD}|^2 + \sigma_D^2} \right\}. \quad (50)$$

Note that the term  $\min \{\cdot, \cdot\}$  in (49) and (50) is introduced by the fixed DF relaying policy applied at R [30]. Knowing  $|h_{SR}|^2 \sim E(\Omega_{SR})$ ,  $|h_{RR}|^2 \sim E(\Omega_{RR})$  and  $|h_{RD}|^2 \sim E(\Omega_{RD})$ , closed-form CDF expressions of  $Y_{\mathcal{H}_0}$  and  $Y_{\mathcal{H}_1}$  can be calculated as

$$F_{Y_{\mathcal{H}_\phi}}(x) = \begin{cases} 1 - \frac{P_S \Omega_{SR} \exp\left(-\left(\frac{\sigma_R^2}{(1-\rho)P_S \Omega_{SR}} + \frac{\sigma_D^2}{P_R \Omega_{RD}}\right)x\right)}{P_S \Omega_{SR} + k P_R \Omega_{RR} x}, & \phi = 0 \\ 1 - \frac{P_S \Omega_{SR} \exp\left(-\left(\frac{\sigma_R^2}{(1-\rho)P_S \Omega_{SR}} + \frac{\sigma_D^2}{(P_R + P_\Delta) \Omega_{RD}}\right)x\right)}{P_S \Omega_{SR} + k (P_R + P_\Delta) \Omega_{RR} x}, & \phi = 1 \& x < \frac{P_R}{P_\Delta} \\ 1, & \phi = 1 \& x \geq \frac{P_R}{P_\Delta} \end{cases}. \quad (51)$$

**Lemma 2:** Closed-form expression of CDF of  $\gamma_D | \mathcal{H}_0$  can be derived as

$$F_{\gamma_D | \mathcal{H}_0}(x) = q_{SD} - v_1 [\text{Ei}(v_3) - \text{Ei}(v_4)] \\ \times \exp \left( \frac{P_S \Omega_{SR} \left( \frac{\sigma_R^2}{(1-\rho)P_S \Omega_{SR}} + \frac{\sigma_D^2}{P_R \Omega_{RD}} \right) - \frac{\sigma_D^2}{P_S \Omega_{SD}} (P_S \Omega_{SR} + k P_R \Omega_{RR} x)}{k P_R \Omega_{RR}} \right), \quad (52)$$

where  $\text{Ei}(\cdot)$  represents the one-argument Exponential Integral function. For concise expression, we define the following variables in (52) as

$$v_1 = \frac{\sigma_D^2 \Omega_{SR}}{k P_R \Omega_{RR} \Omega_{SD}}, \quad (53)$$

$$v_2 = \frac{\frac{\sigma_D^2}{P_S \Omega_{SD}} - \frac{\sigma_R^2}{(1-\rho)P_S \Omega_{SR}} - \frac{\sigma_D^2}{P_R \Omega_{RD}}}{k P_R \Omega_{RR}}, \quad (54)$$

$$v_3 = v_2 (P_S \Omega_{SR} + k P_R \Omega_{RR} x), \quad (55)$$

$$v_4 = v_2 (P_S \Omega_{SR} + k P_R \Omega_{RR} (x - \gamma_{th})). \quad (56)$$

*Proof:* See Appendix E. ■

**Lemma 3:** Closed-form CDF expression of  $\gamma_D | \mathcal{H}_1$  in the case of FD SWIPT mode can be derived approximately as

$$F_{\gamma_D | \mathcal{H}_1}(x) \approx \text{quadgk}(\text{fun}(y), 0, \gamma_{th}), \quad (57)$$

where the definitions of  $\text{quadgk}(\cdot, \cdot, \cdot)$  and  $\text{fun}(y)$  can be found in the following proof.

*Proof:* See Appendix F. ■

**Remark 6:** In **Lemma 3**, the approximation of  $F_{\gamma_D | \mathcal{H}_1}$  is achieved by converting infinite integral to finite summation. The accuracy of this approximation is mainly affected by the amount of nodes used within the finite summation, the more nodes is applied, the more complex the summation is, though the preciser approximation it can achieve.

**Theorem 4:** Closed-form expression of the TOP in the FD SWIPT mode can be given by

$$TOP_{FS} = \frac{1}{2} \sum_{i=\varphi}^L \xi_i [F_{\gamma_D | \mathcal{H}_0}(2^{R_{th}} - 1) + F_{\gamma_D | \mathcal{H}_1}(2^{R_{th}} - 1)]. \quad (58)$$

*Proof:* See Appendix G. ■

**Theorem 5:** Closed-form expression of the TOP in the PEH mode can be given as

$$TOP_{PEH} = q_{SD} \sum_{i=0}^{\varphi-1} \xi_i + F_{\gamma_{SD} | \gamma_{SD} \geq \gamma_{th}}(2^{R_{th}} - 1), \quad (59)$$

where the concept of  $F_{\gamma_{SD} | \gamma_{SD} \geq \gamma_{th}}(x)$  can be found in the following proof.

*Proof:* See Appendix H. ■

**Corollary 3:** Finally, invoking (58) and (59), closed-form expression of overall TOP for our proposed HOR model can be derived as

$$\begin{aligned} TOP &= q_{SD} \sum_{i=0}^{\varphi-1} \xi_i + F_{\gamma_{SD} | \gamma_{SD} \geq \gamma_{th}}(2^{R_{th}} - 1) \\ &\quad + \frac{1}{2} \sum_{i=\varphi}^L \xi_i [F_{\gamma_D | \mathcal{H}_0}(2^{R_{th}} - 1) + F_{\gamma_D | \mathcal{H}_1}(2^{R_{th}} - 1)]. \end{aligned} \quad (60)$$

In this section, the developed closed-form expression of the TOP is indeed in a form of complicated composition, from which the impacts of system parameters on the TOP performance are impossible to be unveiled and discussed thoroughly. To analyse the TOP performance of the

proposed HOR system and thus highlight the superiority of the HOR scheme as well as the impacts of various system parameters on the TOP performance, we pose detailed investigation via showing numerical results in Section VI.

## VI. NUMERICAL RESULTS

In this section, applying the analytical expressions derived in the previous contents, numerical results will be performed and the impact of key parameters on the performance will also be investigated. The simulation is deployed in a 2-dimensional (2D) topology where all the nodes are placed with the same altitude, i.e., terrestrial relaying scenario. Unless otherwise specified, the simulation results are based on the following parameter setups. The distances among nodes are allocated as  $d_{SD} = 15$  m,  $d_{SR} = 8$  m,  $d_{RR} = 0.1$  m and  $d_{RD} = 8$  m, where it is reasonable to consider that the distance between R's dual antennas is relatively near. We set the average wireless channel gains as  $\Omega_{ij} = 1/(1 + d_{ij}^\alpha)$ ,  $\{i,j\} \in \{S, R, D\}$  where the path loss exponent is predefined as  $\alpha = 3$ , the AWGN powers  $\sigma_R^2 = \sigma_D^2 = -60$  dBm, the target transmission rate  $R_{th} = 1$  bps/Hz, the SNR threshold  $\gamma_{th} = 1$ , the energy threshold  $E_{th} = 0.6C_P$ , the transmit power of S  $P_S = -10$  dBm, the PS factor  $\rho = 0.5$  and the covert transmitting power  $P_\Delta = 0.2P_R$ . Regarding parameters of the hybrid energy storage, we set  $C_P = C_M = 10^{-6}$  Joule, the energy conversion efficiency  $\eta = 0.4$ , the energy transfer coefficient  $\eta' = 0.9$  and the discretisation level  $L = 25$ .

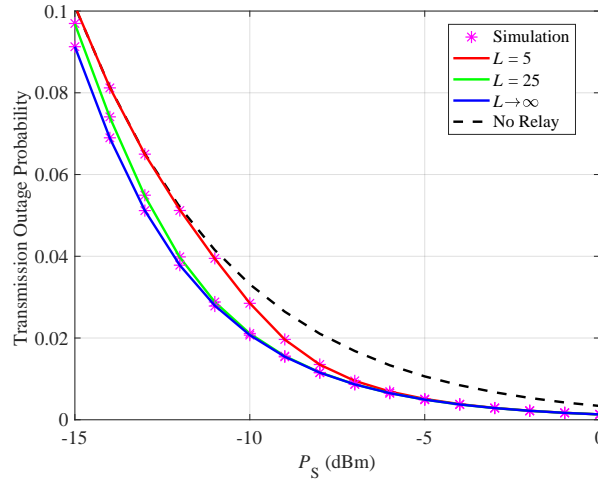


Figure 4. Transmission outage probability versus  $P_S$  with various  $L$  values.

### A. Validation of The Proposed Energy Discretization Method

In this part, we validate the feasibility and accuracy of the proposed discrete energy model described in Section III, by showing curves generated from the MC based TOP analysis and the corresponding Monte Carlo simulation points. Figure 4 depicts curves of the TOP versus  $P_S$  with different energy discretisation levels. Note that  $L \rightarrow \infty$  serves as upper bound of the TOP performance, in the case of a massive energy discretisation. It can be observed from Figure 4 that even a small energy discretisation level ( $L = 5$ ) is enough to provide considerable TOP performance gain for majority of the simulated  $P_S$  regime, compared to the circumstance in which no relay assists wireless communication between S and D. Comparing the TOP performance curves of various  $L$  values, one can conclude that the TOP performance approaches the upper bound gradually as the value of  $L$  increases. The reason why  $L$  can affect the HOR system has been explained in details in **Remark 3**. Specifically, the TOP performance curve when  $L$ 's value is not so large, i.e.,  $L = 25$  can coincide with the upper bound in the most region of simulated  $P_S$ . The aforementioned observations validates the effectiveness of the proposed HOR system on helping wireless transmissions between devices, even with practical energy discretisation levels ( $L = 5, L = 25$ ).

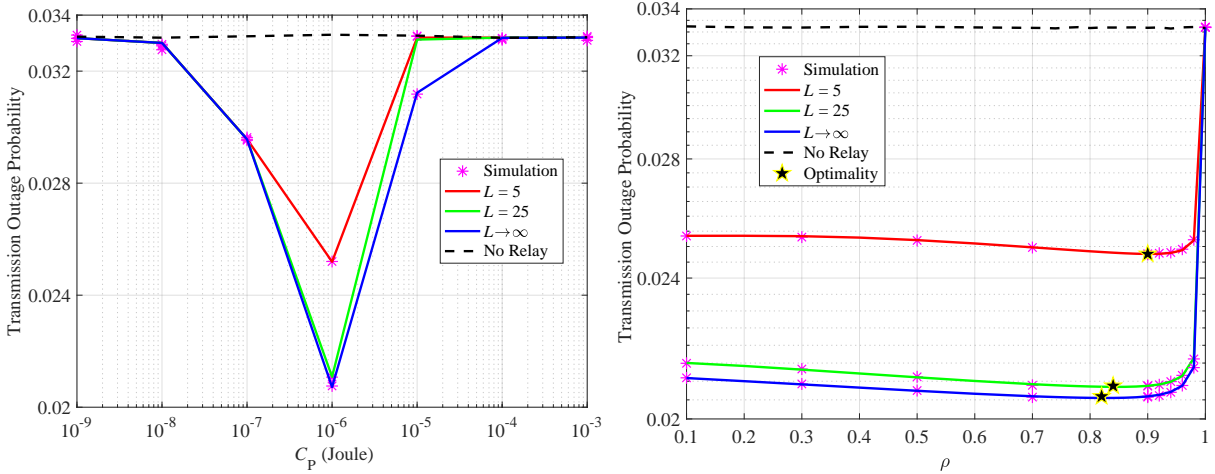


Figure 5. Transmission outage probability versus  $C_P$  with Figure 6. Transmission outage probability versus  $\rho$  with various  $L$  values.

### B. The Impact of Capacity of The PEC

In this subsection, we examine that how  $C_P$  influences the TOP performance. Figure 5 shows the TOP curves versus  $C_P$  with various  $L$  values. It is straightforward to find that for specific HOR system parameter setup, there exists optimal value of  $C_P$  to minimise the TOP performance. The existence of the optimal  $C_P$  is because, briefly speaking, it influences the values of  $P_R$  and  $E_{th}$  by the means of  $P_R = E_{th} = 0.6C_P$ . Under the system parameter setup of this example, the values of  $L$  does not pose any impact on value of the optimal  $C_P$ . It can be observed that  $L = 25$  can almost act as a feasible alternative of the TOP performance's upper bound, revealing the efficiency of the proposed energy discretisation model. The observation of this example allows the system designer to determine an optimal  $C_P$  while reducing computation by selecting a small but sufficient  $L$ , for various system parameter setups.

### C. The Impact of The PS Factor

In this part, we investigate the impact of  $\rho$  on the TOP performance. Figure 6 demonstrates the TOP curves versus  $\rho$  with various  $L$  values. Alongside all the possible values of  $\rho$  towards  $\rho = 1$ , we can find that the TOP curves first decreases, reach the optimality and then rapidly rocket to the worst case at which performance gain offered by the proposed HOR protocol does not exist any more. The existence of the optimality is because the inherent trade-off at R between harvesting more energy and gaining stronger received SNR of the signals from S. Also, one can find that the energy discretisation levels does pose impact on the value of the optimality. Specifically, a larger  $L$  leads to a smaller value of the optimality. It does make sense because a larger  $L$  can reduce the energy loss in the proposed energy discretisation model based on the discussion in **Remark 3** so that R has the space to pose more efforts on information processing.

### D. The Impact of R's AWGN Power

In this subsection, we show the influence of  $\sigma_R^2$  on the TOP performance. Figure 7 depicts the TOP curves versus  $\sigma_R^2$  with various values of  $\rho$ . From the figure, it is straightforward to conclude that the TOP performance is getting worse with the increasing of  $\sigma_R^2$ . Specifically, when R is less or equally "noisy" than D, i.e., in the case of  $\sigma_R^2 \leq \sigma_D^2$ , the TOP performance remains static at the minimum value. On the contrary, a "noisier" R will lead to the loss of performance gain offered by the proposed HOR system. This is because, in short, the min function introduced

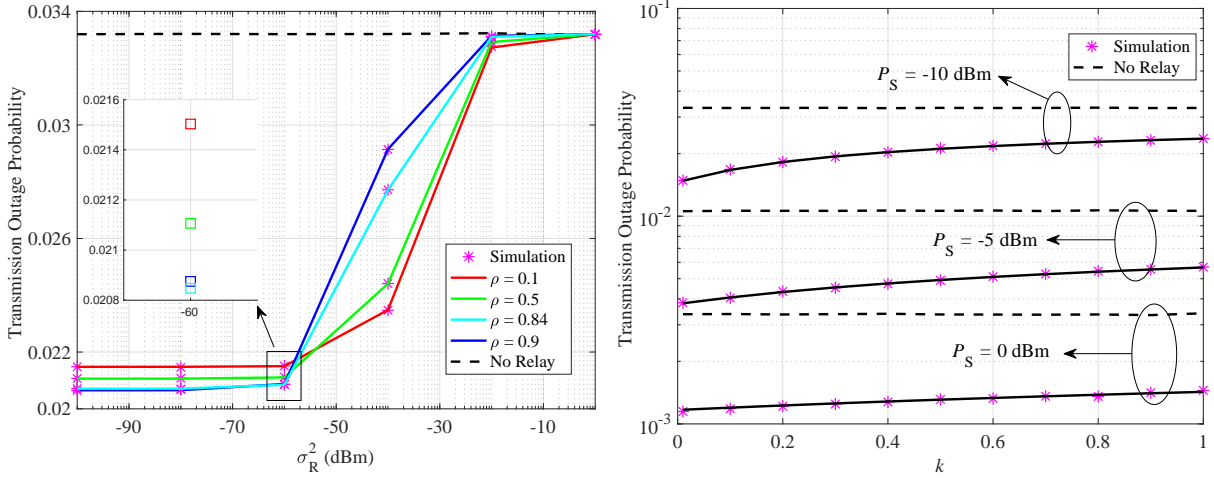


Figure 7. Transmission outage probability versus  $\sigma_R^2$  with Figure 8. Transmission outage probability versus  $k$  with various  $\rho$  values.

by the DF relaying strategy in formulas (49) and (50) forces the overall received SNR  $\gamma_D$  to behave the segmentation feature. Besides, with the increasing of  $\sigma_R^2$ , the impact of  $\rho$  on the TOP performance gradually becomes negligible, e.g., in the case of  $\rho \in [-20, 0]$  dBm. This is because, at this moment,  $Y_{\mathcal{H}_i}, i \in \{0, 1\}$  is way too small compared with  $\gamma_{SD}$ . Moreover, we give the detailed illustration in the case of  $\sigma_R^2 = -60$  dBm. At this point, the TOP performance of  $\rho = 0.84$  (the empirical optimal PS factor from Figure 6) is superior to that of  $\rho = 0.9$ , validating the existing of the optimal  $\rho$  which was found and discussed in the aforementioned Subsection C.

#### E. The Impact of SIC Strength

In this part, we examine how  $k$  can affect the TOP performance. Figure 8 shows the TOP curves versus  $k$  with various  $P_S$  values. It is direct to find from this figure that the TOP performance is becoming worse with the increasing of  $k$ , for all simulated  $P_S$  setups. The reason is that a larger  $k$  means a stronger SI which suppresses the received SNR of R more. Although a larger  $k$  can lead R to harvest more energy from the loop SI channel, from Figure 8, it is still better to pursue a good SIC efficiency, i.e., a smaller value of  $k$ , when implementing the proposed HOR system. Besides, with a higher  $P_S$ , the impact of  $k$  becomes less obvious. This is because the strengths of both energy harvested from the loop SI channel and the interference caused by the



SI link become minor, in the front of a high value of  $P_S$ , which is determined by formulas (8), (49) and (50).

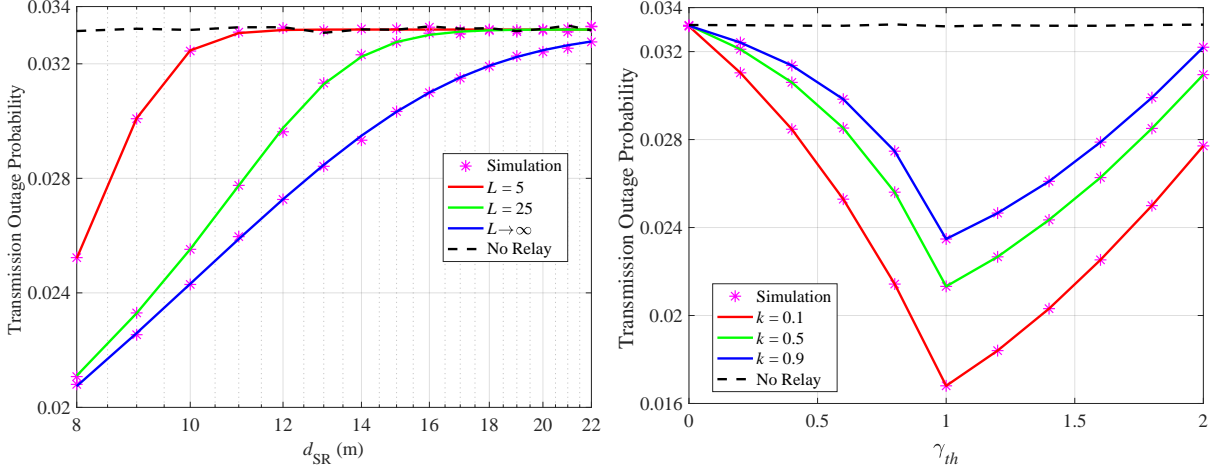


Figure 9. Transmission outage probability versus  $d_{SR}$  with various  $L$  values. Figure 10. Transmission outage probability versus  $\gamma_{th}$  with various  $k$  values.

#### F. The Impact of The Distance Between $S$ and $R$

In this subsection, we discuss the impact of  $d_{SR}$  on the TOP performance. Figure 9 illustrates the TOP curves versus  $d_{SR}$  with various values of  $L$ . Under the subjective of the Triangle Side Length Rule, the possible length of  $d_{SR}$  should locates in  $d_{SR} \in (7, 23)$  m. From Figure 9, it is straightforward to find that no matter what value  $L$  is, a reasonable shorter distance between  $S$  and  $R$  is always preferred for achieving more TOP performance gain. The reason is simply because the amount of harvested energy is very sensitive to  $d_{SR}$ , which can be found in the assumption of  $\Omega_{SR} = 1/(1 + d_{SR}^3)$ . From this figure, the approaching speed of the TOP curves to the “No Relay” line is much slower for a larger  $L$ , validating the discussion in **Remark 3**.

#### G. The Impact of The SNR Threshold

In this part, we analyse how the value of  $\gamma_{th}$  affects the TOP performance. Figure 10 depicts the TOP curves versus  $\gamma_{th}$  with different  $k$  values. From this figure, one can observe that there exists an optimal value of  $\gamma_{th}$  which can minimise the TOP curves. This is because, concisely speaking, the value of  $\gamma_{th}$  directly influences the occurrence frequency of the FD SWIPT mode, which is determined by the activation condition as  $\{\gamma_{SD} < \gamma_{th}\} \cap \{E_i \geq E_{th}\}$ . The dilemma of

“never or less frequently using R” and “using R too much” makes the optimal  $\gamma_{th}$  standing. Besides, the optimal value of  $\gamma_{th}$  is independent to  $k$ . However, a more solid SIC degree, i.e., a smaller  $k$ , is still preferable, which is consistent with the discussion in Subsection E.

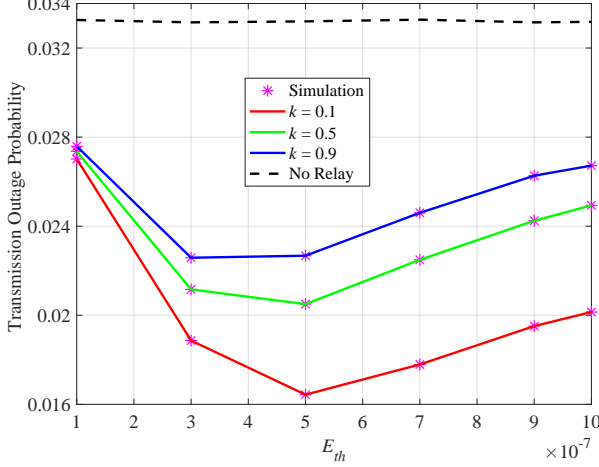


Figure 11. Transmission outage probability versus  $E_{th}$  with various  $k$  values.

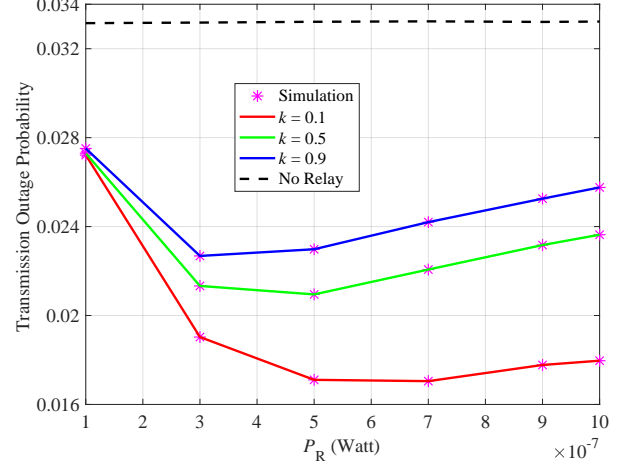


Figure 12. Transmission outage probability versus  $P_R$  with various  $k$  values.

#### H. The Impact of The Energy Threshold

In this subsection, we discuss the impact of  $E_{th}$  on the TOP performance. Figure 11 illustrates the TOP curves versus  $E_{th}$  with various values of  $k$ . It is easy to conclude that an optimal choice of  $E_{th}$  which can minimise the TOP performance does exist for a specific  $k$ . The reason is similar to that discussed in Subsection G, which can be explained by the activation condition of the FD SWIPT mode, i.e.,  $\{\gamma_{SD} < \gamma_{th}\} \cap \{E_i \geq E_{th}\}$ . This observation can help the designer to determine a feasible setup of  $E_{th}$  in practical applications.

#### I. The Impact of R's Transmit Power

In this part, we discuss the impact of  $P_R$  on the TOP performance. Figure 12 depicts the TOP curves versus  $P_R$  with various values of  $k$ . The overall appearance of this figure is similar to that of Figure 11, however the subtle differences can be found by comparing these two figures, illustrating the different influence strengths of  $E_{th}$  and  $P_R$  on the TOP performance. The existence of the optimal  $P_R$  is due to the following two trade-offs: 1) a larger  $P_R$  will consume more stored energy at the PEC but also lead the PEC to absorb more energy from the SI channel. 2) the

min function introduced by the DF relaying strategy limits that  $\gamma_D$  is not always increasing with the increasing of  $P_R$ . This two kinds of dilemma cause that simply enlarging  $P_R$  does not lead to a better TOP performance, and also make the optimal value of  $P_R$  existing. This finding is beneficial for designer to choose a feasible value of  $P_R$  in implement of the proposed HOR system.

## VII. CONCLUSION

In this paper, we initiated a novel wireless relaying transmission scheme termed HOR, via both listing the necessary hardware devices and designing the essential transmission protocol. To realise the SWIPT and true FD functionalities of the proposed HOR system, a practical finite-capacity hybrid energy storage model is applied, which is composed of two independent energy containers. The relay can work opportunistically in either PEH or FD SWIPT mode according to the proposed HOR scheme, not only providing a better way to manipulate available wireless energy but also improving the overall wireless transmission performance within the end-to-end wireless communication scenario. To track the dynamic charge-discharge behaviour of the PEC, a discrete-state MC method is adopted, based on which the long-term stationary distribution of energy states is quantified. Furthermore, covert communication and transmission performances of the proposed HOR system were analysed via deriving closed-form expressions of minimum detection error probability and transmission outage probability. Numerical results validated the correctness of the aforementioned analyses and the impacts of key system parameters were investigated. The proposed HOR scheme can enhance wireless energy manipulating efficiency, wireless transmission performance and privacy level of the end-to-end wireless transmission system, which has been proved throughout this paper.

## APPENDIX A

### PROOF OF LEMMA 1

Under the assumption that D has complete knowledge of his noise power, similar to the proof of Lemma 3 in [31], by applying Fisher-Neyman factorization theorem and Likelihood Ratio ordering, we can prove that radiometer is indeed the optimal choice for D to perform the detection test. The proof details can be stated as follows.

Because each symbol of the received message vector  $\mathbf{y}_D$  in a specific transmission slot follows i.i.d. complex Gaussian distribution,  $\mathbf{y}_D[\omega]$  is ruled by the distribution shown as

$$\begin{cases} \mathcal{CN}\left(0, P_S|h_{SD}|^2 + P_R|\hat{h}_{RD}|^2 + P_R|\tilde{h}_{RD}|^2 + \sigma_D^2\right), & \mathcal{H}_0 \\ \mathcal{CN}\left(0, P_S|h_{SD}|^2 + (P_R + P_\Delta)|\hat{h}_{RD}|^2 + (P_R + P_\Delta)|\tilde{h}_{RD}|^2 + \sigma_D^2\right), & \mathcal{H}_1 \end{cases} \quad (61)$$

Denote the observation conditioned on  $\psi$  by  $\mathbf{y}_D(\psi) = [y_D[1](\psi), y_D[2](\psi), \dots, y_D[n](\psi)]$  in which  $y_D[\omega](\psi) \sim \mathcal{CN}(0, \sigma_D^2 + \psi)$ . Note that  $\psi$  represents the sum variance of D's received signals from S and R. To distinguish the null hypothesis  $\mathcal{H}_0$  from the alternative hypothesis  $\mathcal{H}_1$ , we here introduce a couple of non-negative and real-value RVs  $\Psi_0$  and  $\Psi_1$ , whose PDFs are integrately given by

$$f_{\Psi_q}(\psi) = \begin{cases} \frac{\exp\left(-\frac{\psi - \phi_0}{\beta P_R \Omega_{RD}}\right)}{\beta P_R \Omega_{RD}}, & x > \phi_0, q = 0 \\ \frac{\exp\left(-\frac{\psi - \phi_1}{\beta(P_R + P_\Delta)\Omega_{RD}}\right)}{\beta(P_R + P_\Delta)\Omega_{RD}}, & x > \phi_1, q = 1 \\ 0, & \text{otherwise} \end{cases} \quad (62)$$

where  $\phi_0 = P_S\Omega_{SD} + (1 - \beta)P_R\Omega_{RD}$  and  $\phi_1 = P_S\Omega_{SD} + (1 - \beta)(P_R + P_\Delta)\Omega_{RD}$ .

Furthermore, the PDF of vector  $\mathbf{y}_D$  given  $\psi$  can be calculated as

$$f_{\mathbf{y}_D(\psi)}(\mathbf{y}) = \prod_{\omega=1}^n \frac{\exp\left(-\frac{|\mathbf{y}_D[\omega](\psi)|^2}{\sigma_D^2 + \psi}\right)}{\pi(\sigma_D^2 + \psi)} = \left(\frac{1}{\pi(\sigma_D^2 + \psi)}\right)^n \exp\left(-\frac{\sum_{\omega=1}^n |\mathbf{y}_D[\omega](\psi)|^2}{\sigma_D^2 + \psi}\right). \quad (63)$$

Here, invoking the Fisher-Neyman Factorization Theorem, the total received power in a transmission slot  $\sum_{\omega=1}^n |\mathbf{y}_D[\omega](\psi)|^2$  is a sufficient statistic for D's hypothesis test. It is worth noting that  $\sum_{\omega=1}^n |\mathbf{y}_D[\omega](\psi)|^2 = (\sigma_D^2 + \psi) \mathcal{X}_{2n}^2$  where  $\mathcal{X}_{2n}^2$  denotes chi-squared RV with  $2n$  degrees of freedom. Because D performs testing between two simple hypotheses and he knows the statistical knowledge of his received signals when either hypothesis stands, with help of the Neyman-Pearson Lemma, the best testing rule for D to decide which hypothesis stands is the likelihood ratio test (LRT), given by

$$\Lambda(\mathbf{y}_D) = \frac{f_{\mathbf{y}_D|\mathcal{H}_1}(\mathbf{y})}{f_{\mathbf{y}_D|\mathcal{H}_0}(\mathbf{y})} \underset{\mathcal{D}_0}{\overset{\mathcal{D}_1}{\gtrless}} \Gamma, \quad (64)$$

where  $\Gamma = \Pr(\mathcal{H}_1) / \Pr(\mathcal{H}_0) = 1$  due to the application of equal *a priori* assumption. D does not have instantaneous knowledge of either  $\Psi_0$  or  $\Psi_1$ , so he modifies his LRT as

$$\Lambda(\mathbf{y}_D) = \frac{\mathbb{E}_{\Psi_1}[f_{\mathbf{y}_D(\psi)}(\mathbf{y})]}{\mathbb{E}_{\Psi_0}[f_{\mathbf{y}_D(\psi)}(\mathbf{y})]} \underset{\mathcal{D}_0}{\overset{\mathcal{D}_1}{\gtrless}} \Gamma. \quad (65)$$

We introduce here that RV  $X$  is smaller than RV  $Y$  in the likelihood ratio order, i.e.,  $X \leq_{lr} Y$ , when  $f_Y(x)/f_X(x)$  is an non-decreasing function over the union of their supports.

Invoking (62), we have

$$\frac{f_{\Psi_1}(\psi)}{f_{\Psi_0}(\psi)} = \frac{P_R}{P_R + P_\Delta} \exp\left(\frac{P_\Delta \psi - (P_R + P_\Delta) \phi_0 + P_R \phi_1}{\beta P_R (P_R + P_\Delta) \Omega_{RD}}\right). \quad (66)$$

It is straightforward to find that (66) is non-decreasing over the union of supports of  $\Psi_0$  and  $\Psi_1$ , hence  $\Psi_0 \leq_{lr} \Psi_1$ . From the statistical nature of chi-squared RVs, for any  $\psi_1 \leq \psi_2$ , we have  $\mathbf{y}_D(\psi_1) \leq_{lr} \mathbf{y}_D(\psi_2)$ . Then, according to Theorem 1, Chapter 11 in [32], the monotonicity of  $\Lambda(\mathbf{y}_D)$  is ruled by Stochastic Ordering and  $\Lambda(\mathbf{y}_D)$  is non-decreasing w.r.t.  $\sum_{\omega=1}^n |\mathbf{y}_D[\omega](\psi)|^2$ . Hence, the LRT (65) is equivalent to a received power threshold test. Since any one-to-one transformation of a sufficient statistic remains the sufficiency, the term  $\sum_{\omega=1}^n |\mathbf{y}_D[\omega]|^2/n$  is also a sufficient statistic. From the strong law of large numbers, we have  $\mathcal{X}_{2n}^2/n \rightarrow 1$  when infinite blocklength ( $n \rightarrow \infty$ ) assumption is considered. Invoking the Lebesgue's Dominated Convergence Theorem, it is allowed to replace  $\mathcal{X}_{2n}^2/n$  by 1, when  $n \rightarrow \infty$ . Thus, we get

$$\begin{aligned} T &= \lim_{n \rightarrow \infty} \frac{1}{n} \sum_{\omega=1}^n |\mathbf{y}_D[\omega]|^2 \\ &= \begin{cases} P_S |h_{SD}|^2 + P_R |\hat{h}_{RD}|^2 + P_R |\tilde{h}_{RD}|^2 + \sigma_D^2, & \mathcal{H}_0 \\ P_S |h_{SD}|^2 + (P_R + P_\Delta) |\hat{h}_{RD}|^2 + (P_R + P_\Delta) |\tilde{h}_{RD}|^2 + \sigma_D^2, & \mathcal{H}_1 \end{cases}. \end{aligned} \quad (67)$$

Then, the optimal decision rule at D can be expressed as

$$T \underset{\mathcal{D}_0}{\overset{\mathcal{D}_1}{\geq}} \tau,$$

where  $\tau$  denotes the threshold which will be optimized to minimize  $\mathbb{P}_E$ .

After all, a radiometer which is able to detect the total power of received messages at D is proved to be optimal. Besides, radiometers are also beneficial for D due to its low complexity and ease of implementation. So, it is sufficient and optimal for D to apply a radiometer to perform hypothesis test regarding covert communication detection.

## APPENDIX B

### PROOF OF THEOREM 2

Based on (67), we can calculate the false alarm and missed detection probabilities, given respectively by

$$\mathbb{P}_{FA} = \Pr(T > \tau | \mathcal{H}_0) = \Pr\left(P_R |\tilde{h}_{RD}|^2 + j_0 > \tau\right) = \begin{cases} \Pr\left(|\tilde{h}_{RD}|^2 > \frac{\tau - j_0}{P_R}\right), & \tau \geq j_0 \\ 1, & \text{otherwise} \end{cases}, \quad (68)$$

$$\begin{aligned}
\mathbb{P}_{\text{MD}} &= \Pr(T < \tau | \mathcal{H}_1) \\
&= \Pr\left((P_{\text{R}} + P_{\Delta}) |\tilde{h}_{\text{RD}}|^2 + j_1 < \tau\right) = \begin{cases} \Pr\left(|\tilde{h}_{\text{RD}}|^2 < \frac{\tau - j_1}{P_{\text{R}} + P_{\Delta}}\right), & \tau \geq j_1 \\ 0, & \text{otherwise} \end{cases}. \quad (69)
\end{aligned}$$

Because the uncertain part of channel  $\text{R} \rightarrow \text{D}$  follows the distribution  $\tilde{h}_{\text{RD}} \sim \mathcal{CN}(0, \beta\Omega_{\text{RD}})$ , it is straightforward to know that  $|\tilde{h}_{\text{RD}}|^2$  obeys the Exponential distribution. Thus, the CDF of  $|\tilde{h}_{\text{RD}}|^2$  can be gained as  $F_{|\tilde{h}_{\text{RD}}|^2}(x) = 1 - \exp(-x/(\beta\Omega_{\text{RD}}))$ . Then, after some simple algebra calculation, we gain closed-form expressions of false alarm and missed detection probabilities, expressed respectively as (42) and (43). Invoking (40), (42) and (43), closed-form expression of detection error probability can be gained after simple derivation as (44).

## APPENDIX C

### PROOF OF THEOREM 3

To determine the optimal detection threshold of D's radiometer, it is supposed to solve the following optimization problem, shown as

$$\tau^* = \arg \min_{\tau} \mathbb{P}_{\text{E}}. \quad (70)$$

In the case of  $\tau < j_0$ , the detection error probability at D remains 1. This is the worst case for D and D will never choose any value satisfying  $\tau < j_0$ . Thus, the optimization problem did not stand in this case.

In the case of  $j_0 \leq \tau < j_1$ , it is easy to find that  $\mathbb{P}_{\text{E}}$  monotonically decreases w.r.t.  $\tau$ . Besides, the piecewise function  $\mathbb{P}_{\text{E}}$  is a continuous function along side the whole feasible domain of  $\tau$ . Thus, D will choose  $j_1$  to minimize  $\mathbb{P}_{\text{E}}$ , leading to  $\mathbb{P}_{\text{E}} = \exp((j_0 - j_1)/(\beta P_{\text{R}} \Omega_{\text{RD}}))$ .

In the case of  $\tau \geq j_1$ , to determine the optimal value of  $\tau$ , the first derivative of function  $\mathbb{P}_{\text{E}}$  w.r.t.  $\tau$  is calculated as

$$\frac{\partial \mathbb{P}_{\text{E}}}{\partial \tau} = \frac{k}{\beta P_{\text{R}} (P_{\text{R}} + P_{\Delta}) \Omega_{\text{RD}}}, \quad (71)$$

where  $k = P_{\text{R}} \exp[(j_1 - \tau)/(\beta(P_{\text{R}} + P_{\Delta})\Omega_{\text{RD}})] - (P_{\text{R}} + P_{\Delta}) \exp[(j_0 - \tau)/(\beta P_{\text{R}} \Omega_{\text{RD}})]$ . It is easy to find that whether (71) is positive or not depends only on the value of  $k$ . After simple manipulations, we can modify  $k$  as

$$k = \exp\left(\ln P_{\text{R}} + \frac{j_1 - \tau}{\beta(P_{\text{R}} + P_{\Delta})\Omega_{\text{RD}}}\right) - \exp\left(\ln(P_{\text{R}} + P_{\Delta}) + \frac{j_0 - \tau}{\beta P_{\text{R}} \Omega_{\text{RD}}}\right). \quad (72)$$

Besides, the Exponential function  $\exp$  is monotonically increasing w.r.t. the feasible independent variable region. Thus, we can determine whether  $k$  is positive or not by

$$\begin{aligned} k_1 &= \ln \frac{P_R}{P_R + P_\Delta} + \frac{P_R (j_1 - \tau) - (P_R + P_\Delta) (j_0 - \tau)}{\beta P_R (P_R + P_\Delta) \Omega_{RD}} \\ &= \ln \frac{P_R}{P_R + P_\Delta} + \frac{P_\Delta (\tau - P_S |h_{SD}|^2 - \sigma_D^2)}{\beta P_R (P_R + P_\Delta) \Omega_{RD}}. \end{aligned} \quad (73)$$

Because  $\tau \geq j_1$  stands in this considered case, the right hand of (73) is absolutely positive. However, the left hand of (73) is negative due to  $P_R < P_R + P_\Delta$ . Most importantly, from (73), we can find that  $k_1$  is a monotonically increasing function w.r.t.  $\tau$ . Let  $k_1 = 0$ , we can get the solution as (46). From (46), we can conclude that  $k_1 \geq 0$  in the case of  $\tau \geq \tau_{k_1=0}$  and  $k_1 < 0$  otherwise. If  $j_1 \geq \tau_{k_1=0}$  holds, in the case of  $\tau \geq j_1$ , we can determine that  $k > 0$  and furthermore  $\partial \mathbb{P}_E / \partial \tau > 0$  which means  $\mathbb{P}_E$  monotonically increases w.r.t.  $\tau$  when  $\tau \geq j_1$ . Here, it is the optimal choice for D to choose  $j_1$  as the optimal threshold which is able to minimize  $\mathbb{P}_E$ . If  $j_1 < \tau_{k_1=0}$ , we know that for  $\tau \in (j_1, \tau_{k_1=0})$ ,  $\partial \mathbb{P}_E / \partial \tau < 0$  and for  $\tau \in (\tau_{k_1=0}, +\infty)$ ,  $\partial \mathbb{P}_E / \partial \tau > 0$ . Thus, the optimal detection threshold for D is  $\tau_{k_1=0}$  in this case.

## APPENDIX D

### PROOF OF COROLLARY 2

In the case of  $j_1 \geq \tau_{k_1=0}$ , i.e.,  $\beta \geq -P_\Delta |\hat{h}_{RD}|^2 / \left( P_R \Omega_{RD} \ln \frac{P_R}{P_R + P_\Delta} \right)$ , the first derivative of  $\mathbb{P}_E^*$  w.r.t.  $\beta$  can be calculated as

$$\frac{\partial \mathbb{P}_E^*}{\partial \beta} \Big|_{j_1 \geq \tau_{k_1=0}} = -\frac{j_0 - j_1}{\beta^2 P_R \Omega_{RD}} \exp \left( \frac{j_0 - j_1}{\beta P_R \Omega_{RD}} \right), \quad (74)$$

whose value is positive due to  $j_0 < j_1$ . For  $j_1 < \tau_{k_1=0}$ , i.e.,  $\beta < -P_\Delta |\hat{h}_{RD}|^2 / \left( P_R \Omega_{RD} \ln \frac{P_R}{P_R + P_\Delta} \right)$ , the first derivative of  $\mathbb{P}_E^*$  w.r.t.  $\beta$  can be calculated as

$$\begin{aligned} \frac{\partial \mathbb{P}_E^*}{\partial \beta} \Big|_{j_1 < \tau_{k_1=0}} &= \frac{|\hat{h}_{RD}|^2}{\beta^2 \Omega_{RD}} \\ &\times \left[ \exp \left( \frac{|\hat{h}_{RD}|^2}{\beta^2 \Omega_{RD}} + \frac{P_R}{P_\Delta} \ln \frac{P_R}{P_R + P_\Delta} \right) - \exp \left( \frac{|\hat{h}_{RD}|^2}{\beta^2 \Omega_{RD}} + \frac{P_R + P_\Delta}{P_\Delta} \ln \frac{P_R}{P_R + P_\Delta} \right) \right], \end{aligned} \quad (75)$$

whose value is also positive due to the truth of  $P_R > P_\Delta > 0$ . Thus, we can conclude that  $\mathbb{P}_E^*$  monotonically increases as  $\beta$  increases.

## APPENDIX E

### PROOF OF LEMMA 2

The CDF of  $\gamma_D|\mathcal{H}_0$  can be constructed as

$$F_{\gamma_D|\mathcal{H}_0}(x) = \Pr\left(\gamma_{SD} + Y_{\mathcal{H}_0} < x \bigcap \gamma_{SD} < \gamma_{th}\right). \quad (76)$$

Note that the limitation of variable  $\gamma_{SD}$  should be constrained as  $\gamma_{SD} < \gamma_{th}$  due to the nature of FD SWIPT mode. Invoking (51) and after some simple mathematical computation, we can earn closed-form expression of (76) as (52).

## APPENDIX F

### PROOF OF LEMMA 3

Closed-form CDF expression of  $\gamma_D|\mathcal{H}_1$  should be calculated in the way similar to the derivation of (52). However, we found that it is mathematically intractable. To tackle this problem, we resort to Gauss-Kronrod Quadrature (GKQ) method to approximately solve it, shown as

$$\begin{aligned} F_{\gamma_D|\mathcal{H}_1}(x) &= \Pr\left[\gamma_{SD} + Y_{\mathcal{H}_1} < x \bigcap \gamma_{SD} < \gamma_{th}\right] \\ &= \int_0^{\gamma_{th}} \underbrace{\frac{\sigma_D^2}{P_S \Omega_{SD}} F_{Y_{\mathcal{H}_1}}(x - y) \exp\left(-\frac{\sigma_D^2 y}{P_S \Omega_{SD}}\right)}_{\text{fun}} dy \\ &\approx \sum_{i=1}^n \varrho_i \text{fun}(y_i), \end{aligned} \quad (77)$$

where  $\varrho_i$  and  $y_i$  denote the weights and points which are essential to evaluate the function  $\text{fun}(y)$ . Note that the GKQ formula is an adaptive method for numerical integration, which is a variant of Gaussian quadrature. In this paper, we use the built-in function of Matlab named `quadgk`( $\cdot, \cdot, \cdot$ ) to calculate (77), which implements adaptive quadrature based on a Gauss-Kronrod pair (15<sup>th</sup> and 7<sup>th</sup> order formulas). Applying `quadgk`( $\cdot, \cdot, \cdot$ ), we can derive closed-form approximate CDF expression of  $\gamma_D|\mathcal{H}_1$  as (57).



APPENDIX G  
PROOF OF THEOREM 4

In our considered HOR model, the TOP in the case of FD SWIPT should be constructed as

$$\begin{aligned}
 TOP_{\text{FS}} &= \Pr \left[ \log_2 (1 + \gamma_{\text{D}}) < R_{th} \bigcap \mathcal{H}_0 \bigcap \text{FS} \right] + \Pr \left[ \log_2 (1 + \gamma_{\text{D}}) < R_{th} \bigcap \mathcal{H}_1 \bigcap \text{FS} \right] \\
 &\stackrel{a}{=} \Pr \left[ \log_2 (1 + \gamma_{\text{D}}) < R_{th} \bigcap \mathcal{H}_0 \bigcap \gamma_{\text{SD}} < \gamma_{th} \right] \sum_{i=\varphi}^L \xi_i + \\
 &\Pr \left[ \log_2 (1 + \gamma_{\text{D}}) < R_{th} \bigcap \mathcal{H}_1 \bigcap \gamma_{\text{SD}} < \gamma_{th} \right] \sum_{i=\varphi}^L \xi_i \\
 &= \frac{1}{2} \sum_{i=\varphi}^L \xi_i \\
 &\times \left\{ \underbrace{\Pr \left[ \gamma_{\text{D}} | \mathcal{H}_0 < 2^{R_{th}} - 1 \bigcap \gamma_{\text{SD}} < \gamma_{th} \right]}_{f_1} + \underbrace{\Pr \left[ \gamma_{\text{D}} | \mathcal{H}_1 < 2^{R_{th}} - 1 \bigcap \gamma_{\text{SD}} < \gamma_{th} \right]}_{f_2} \right\}, \tag{78}
 \end{aligned}$$

where the factor  $1/2$  is due to the assumption of equal *a priori*,  $R_{th}$  is the target rate under which the transmission outage occurs. Note that step (a) in (78) holds, because of the fact that the energy requirement is independent with other factors. With the help of **Lemma 2** and **Lemma 3**, we are able to derive closed-form expressions of  $f_1$  and  $f_2$ , which can be achieved by simply replacing variable  $x$  in (52) and (57) with factor  $2^{R_{th}} - 1$ . Substituting  $f_1$  and  $f_2$  into (78), we can derive closed-form expression of the TOP in the FD SWIPT mode as (58) and this completes the proof.

APPENDIX H  
PROOF OF THEOREM 5

Similar to the derivation of (58), in the PEH mode, the TOP should be constructed as

$$\begin{aligned}
 TOP_{\text{PEH}} &= \Pr \left[ \log_2 (1 + \gamma_{\text{D}}) < R_{th} \bigcap \text{PEH} \right] \\
 &= \underbrace{\Pr \left( \gamma_{\text{SD}} < 2^{R_{th}} - 1 \bigcap \gamma_{\text{SD}} < \gamma_{th} \right)}_{f_3} \sum_{i=0}^{\varphi-1} \xi_i + \underbrace{\Pr \left( \gamma_{\text{SD}} < 2^{R_{th}} - 1 \bigcap \gamma_{\text{SD}} \geq \gamma_{th} \right)}_{f_4}. \tag{79}
 \end{aligned}$$

In the case of  $\gamma_{\text{SD}} < \gamma_{th} \cap E_i < E_{th}$ , we have  $\Pr (\gamma_{\text{SD}} < 2^{R_{th}} - 1) = 1$ . It is worth noting that hereby  $\Pr (\gamma_{\text{SD}} < 2^{R_{th}} - 1)$  and  $\Pr (\gamma_{\text{SD}} < \gamma_{th})$  are independent with each other, because D

cases signal-processing and forces  $\Pr(\gamma_{SD} < 2^{R_{th}} - 1) = 1$ , leading  $f_3 = \Pr(\gamma_{SD} < \gamma_{th}) = q_{SD}$ . In the case of  $\gamma_{SD} \geq \gamma_{th}$ , the main wireless channel is good enough, closed-form expression of CDF of  $\gamma_{SD} | \gamma_{SD} \geq \gamma_{th}$  can be derive as

$$F_{\gamma_{SD} | \gamma_{SD} \geq \gamma_{th}}(x) = \begin{cases} \exp\left(-\frac{\sigma_D^2 \gamma_{th}}{P_S \Omega_{SD}}\right) - \exp\left(-\frac{\sigma_D^2 x}{P_S \Omega_{SD}}\right), & x > \gamma_{th} \\ 0, & x \leq \gamma_{th} \end{cases}. \quad (80)$$

Hence, closed-form expression of  $f_4$  can be given by  $f_4 = F_{\gamma_{SD} | \gamma_{SD} \geq \gamma_{th}}(2^{R_{th}} - 1)$ . Substituting  $f_3$  and  $f_4$  into (79), we can derive closed-form expression of the TOP in the PEH mode as (59) and this completes the proof.

## REFERENCES

- [1] Y. Bi and H. Chen, "Accumulate and jam: Towards secure communication via a wireless-powered full-duplex jammer," *IEEE J. Sel. Signal Process.*, vol. 10, no. 8, pp. 1538–1550, 2016.
- [2] Z. Chu, F. Zhou, P. Xiao, Z. Zhu, D. Mi, N. Al-Dhahir, and R. Tafazolli, "Resource allocation for secure wireless powered integrated multicast and unicast services with full duplex self-energy recycling," *IEEE Trans. Wireless Commun.*, vol. 18, no. 1, pp. 620–636, 2018.
- [3] L. R. Varshney, "Transporting information and energy simultaneously," in *Proc. IEEE Int. Symp. Inf. Theory (ISIT)*, Toronto, Canada, Jul. 2008.
- [4] R. Zhang and C. K. Ho, "MIMO broadcasting for simultaneous wireless information and power transfer," *IEEE Trans. Wireless Commun.*, vol. 12, no. 5, pp. 1989–2001, May 2013.
- [5] I. Krikidis, "Simultaneous information and energy transfer in large-scale networks with/without relaying," *IEEE Trans. Commun.*, vol. 62, no. 3, pp. 900–912, Mar. 2014.
- [6] J. Yan and Y. Liu, "A dynamic SWIPT approach for cooperative cognitive radio networks," *IEEE Trans. Veh. Technol.*, vol. 66, no. 12, pp. 11 122–11 136, Dec. 2017.
- [7] H. Zhang, J. Du, J. Cheng, K. Long, and V. C. Leung, "Incomplete CSI based resource optimization in SWIPT enabled heterogeneous networks: A non-cooperative game theoretic approach," *IEEE Trans. Wireless Commun.*, vol. 17, no. 3, pp. 1882–1892, Mar. 2018.
- [8] J. Rostampoor, S. M. Razavizadeh, and I. Lee, "Energy efficient precoding design for SWIPT in MIMO two-way relay networks," *IEEE Trans. Veh. Technol.*, vol. 66, no. 9, pp. 7888–7896, Sep. 2017.
- [9] Z. Chen, T. Q. Quek, and Y.-C. Liang, "Spectral efficiency and relay energy efficiency of full-duplex relay channel," *IEEE Trans. Wireless Commun.*, vol. 16, no. 5, pp. 3162–3175, May 2017.
- [10] P. Xing, J. Liu, C. Zhai, X. Wang, and X. Zhang, "Multipair two-way full-duplex relaying with massive array and power allocation," *IEEE Trans. Veh. Technol.*, vol. 66, no. 10, pp. 8926–8939, Oct. 2017.
- [11] Y. Li, R. Zhao, L. Fan, and A. Liu, "Antenna mode switching for full-duplex destination-based jamming secure transmission," *IEEE Access*, vol. 6, pp. 9442–9453, Mar. 2018.
- [12] E. Ahmed and A. M. Eltawil, "All-digital self-interference cancellation technique for full-duplex systems," *IEEE Trans. Wireless Commun.*, vol. 14, no. 7, pp. 3519–3532, Jul. 2015.
- [13] C. Li, Z. Chen, Y. Wang, Y. Yao, and B. Xia, "Outage analysis of the full-duplex decode-and-forward two-way relay system," *IEEE Trans. Veh. Technol.*, vol. 66, no. 5, pp. 4073–4086, May 2017.

- [14] S. Sohaib and M. Uppal, "Full duplex compress-and-forward relaying under residual self-interference," *IEEE Trans. Veh. Technol.*, vol. 67, no. 3, pp. 2776–2780, Mar. 2017.
- [15] M. M. Razlighi and N. Zlatanov, "Buffer-aided relaying for the two-hop full-duplex relay channel with self-interference," *IEEE Trans. Wireless Commun.*, vol. 17, no. 1, pp. 477–491, Jan. 2018.
- [16] Q. Wang, Y. Dong, X. Xu, and X. Tao, "Outage probability of full-duplex AF relaying with processing delay and residual self-interference," *IEEE Commun. Lett.*, vol. 19, no. 5, pp. 783–786, May 2015.
- [17] Y. Li, R. Zhao, X. Tan, and Z. Nie, "Secrecy performance analysis of artificial noise aided precoding in full-duplex relay systems," in *Proc. IEEE GLOBECOM*, Dec. 2017, pp. 1–6.
- [18] B. A. Bash, D. Goeckel, and D. Towsley, "Limits of reliable communication with low probability of detection on awgn channels," *IEEE J. Sel. Areas Commun.*, vol. 31, no. 9, pp. 1921–1930, 2013.
- [19] K. Shahzad, X. Zhou, S. Yan, J. Hu, F. Shu, and J. Li, "Achieving covert wireless communications using a full-duplex receiver," *IEEE Trans. Wireless Commun.*, vol. 17, no. 12, pp. 8517–8530, 2018.
- [20] T.-X. Zheng, H.-M. Wang, D. W. K. Ng, and J. Yuan, "Multi-antenna covert communications in random wireless networks," *IEEE Trans. Wireless Commun.*, vol. 18, no. 3, pp. 1974–1987, 2019.
- [21] X. Zhou, S. Yan, J. Hu, J. Sun, J. Li, and F. Shu, "Joint optimization of a uav's trajectory and transmit power for covert communications," *IEEE Trans. Signal Process.*, vol. 67, no. 16, pp. 4276–4290, 2019.
- [22] D. Wang, R. Zhang, X. Cheng, L. Yang, and C. Chen, "Relay selection in full-duplex energy-harvesting two-way relay networks," *IEEE Trans. Green Commun. Netw.*, vol. 1, no. 2, pp. 182–191, Jun. 2017.
- [23] Z. Wen, X. Liu, N. C. Beaulieu, and R. Wang, "Joint source and relay beamforming design for full-duplex MIMO AF relay SWIPT systems," *IEEE Commun. Lett.*, vol. 20, no. 2, pp. 320–323, 2016.
- [24] Y. Zeng and R. Zhang, "Full-duplex wireless-powered relay with self-energy recycling," *IEEE Wireless Commun. Lett.*, vol. 4, no. 2, pp. 201–204, 2015.
- [25] H. Liu, K. J. Kim, K. S. Kwak, and H. V. Poor, "Power splitting-based swipt with decode-and-forward full-duplex relaying," *IEEE Trans. Wireless Commun.*, vol. 15, no. 11, pp. 7561–7577, 2016.
- [26] J. Hu, S. Yan, F. Shu, and J. Wang, "Covert transmission with a self-sustained relay," *IEEE Trans. Wireless Commun.*, vol. 18, no. 8, pp. 4089–4102, 2019.
- [27] J. Wang, W. Tang, Q. Zhu, X. Li, H. Rao, and S. Li, "Covert communication with the help of relay and channel uncertainty," *IEEE Wireless Commun. Lett.*, vol. 8, no. 1, pp. 317–320, 2018.
- [28] K. Shahzad, "Relaying via cooperative jamming in covert wireless communications," in *2018 12th International Conference on Signal Processing and Communication Systems (ICSPCS)*. IEEE, 2018, pp. 1–6.
- [29] I. Krikidis, T. Charalambous, and J. S. Thompson, "Buffer-aided relay selection for cooperative diversity systems without delay constraints," *IEEE Trans. Wireless Commun.*, vol. 11, no. 5, pp. 1957–1967, 2012.
- [30] R. Zhao, Y. Yuan, L. Fan, and Y.-C. He, "Secrecy performance analysis of cognitive decode-and-forward relay networks in nakagami- $m$  fading channels," *IEEE Trans. Commun.*, vol. 65, no. 2, pp. 549–563, 2016.
- [31] T. V. Sobers, B. A. Bash, S. Guha, D. Towsley, and D. Goeckel, "Covert communication in the presence of an uninformed jammer," *IEEE Trans. Wireless Commun.*, vol. 16, no. 9, pp. 6193–6206, 2017.
- [32] M. Shaked and J. G. Shanthikumar, "Stochastic orders and their applications. 1994," *Acad-emic Press, New York*.